crystals

MDPI

Review

Graphene to Advanced MoS_2: A Review of Structure, Synthesis, and Optoelectronic Device Application

Tahreem Nawz [1], Amna Safdar [1,*], Muzammil Hussain [2], Dae Sung Lee [2] and Muhammad Siyar [1]

1 Department of Materials Engineering, School of Chemical and Materials Engineering, National University of Sciences and Technology, H-12 Islamabad 44000, Pakistan; tnawz.nse6@scme.nust.edu.pk (T.N.); muhammad.siyar@scme.nust.edu.pk (M.S.)

2 Department of Environmental Engineering, Kyungpook National University, Daegu 41566, Korea; muzammil@knu.ac.kr (M.H.); daesung@knu.ac.kr (D.S.L.)

* Correspondence: amna.safdar@scme.nust.edu.pk

Received: 29 June 2020; Accepted: 3 August 2020; Published: 6 October 2020

check for updates

Abstract: In contrast to zero-dimensional (0D), one-dimensional (1D), and even their bulk equivalents, in two-dimensional (2D) layered materials, charge carriers are confined across thickness and are empowered to move across the planes. The features of 2D structures, such as quantum confinement, high absorption coefficient, high surface-to-volume ratio, and tunable bandgap, make them an encouraging contestant in various fields such as electronics, energy storage, catalysis, etc. In this review, we provide a gentle introduction to the 2D family, then a brief description of transition metal dichalcogenides (TMDCs), mainly focusing on MoS_2, followed by the crystal structure and synthesis of MoS_2, and finally wet chemistry methods. Later on, applications of MoS_2 in dye-sensitized, organic, and perovskite solar cells are discussed. MoS_2 has impressive optoelectronic properties; due to the fact of its tunable work function, it can be used as a transport layer, buffer layer, and as an absorber layer in heterojunction solar cells. A power conversion efficiency (PCE) of 8.40% as an absorber and 13.3% as carrier transfer layer have been reported for MoS_2-based organic and perovskite solar cells, respectively. Moreover, MoS_2 is a potential replacement for the platinum counter electrode in dye-sensitized solar cells with a PCE of 7.50%. This review also highlights the incorporation of MoS_2 in silicon-based heterostructures where graphene/MoS_2/n-Si-based heterojunction solar cell devices exhibit a PCE of 11.1%.

Keywords: 2D materials; heterostructure solar cells; MoS_2; graphene

1. Introduction

The house of 2D layered materials [1] has gained appreciable attention over the last few years, starting with the first segregation of graphene from a bulk counterpart, i.e., graphite [2]. The disclosure of every new material leads to enthusiasm and mystery because of the contrasting properties of these 2D materials from their bulk counterparts. Moreover, the fascinating 2D library is increasing in size every year and attributes a surplus of 150 exotic materials that can easily be cleaved into sub-nanometer 2D monolayers [3–6]. These 2D materials [7] include transition metal dichalcogenides (TMDCs), e.g., WSe_2, MoS_2, WS_2, hexagonal boron nitride (h-BN), silicene (2D silicone), germanen (2D germanium), borophene (2D boron), and MXenes (2D carbides/nitrides) [8–11]. In Figure 1, a publication list of 2D materials charted by year depicts an intensified craze of probing TMDCs.

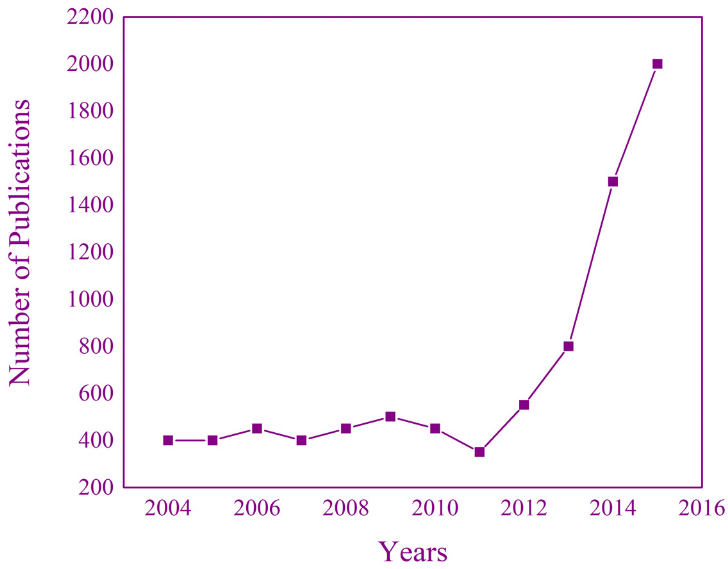

Figure 1. The number of publications for 2D materials reporting from 2004 to 2014 [12].

Two-dimensional layered materials are highly crystalline and have an elevated ratio of their lateral size (1~10,000 µm) to the thickness value (<1 nm) [13]. Two-dimensional materials have a layered structure with strong covalent intralayer bonding and relatively delicate interlayer van der Waals forces [3]. The layered structure of 2D materials permits efficient electronic properties and conductivity is prevalent along with the layers than between the layers, normally three or four folds of magnitude [13–15]. The disclosure of graphene and its distinctive properties in 2004 [16] introduced scientific insurgency where afterward a large number of more layered materials were exfoliated in 2D structures in a combination of elements highlighted in Figure 2a.

Graphene protruded from the other 2D materials because of its quirky properties like exclusive electronic band structure, high transparency with 0 eV bandgap, and thermal conductivity (3000–5000 $Wm^{-1}K^{-1}$) [17]. These unique properties enabled graphene to be a significant applicant in place of indium tin oxide (ITO)—that is transparent conductive oxide (TCO) thoughtfully applied in liquid crystal displays and LEDs, etc. Indium Tin Oxide (ITO) lost its performance due to the fact of flexibility shortfall and insufficient indium [18].

However graphene is a semimetal with zero bandgap, and in this scenario, one can say that other 2D materials, particularly TMDCs, have what graphene does not: a bandgap range of 1.2 to 1.8 eV [19], which admirably corresponds to solar spectrum and analogs to ongoing industrial needs in photovoltaic, e.g., Si (1.1 eV), CdTe (1.5 eV) or GaAs (1.4 eV). The upcoming generations of nanoelectronics require a discourse of the enhancing desire of reducing the size of elements in the circuit but not the quality. Due to the usage of monoatomic thin layers of 2D materials and their fine quality, it is possible to control electrostatic conductivity more efficiently. Moreover, the charge carrier scattering is reduced in 2D materials as compared to their bulk counterpart, owing to the reduced number of dandling bonds [20]. Two-dimensional materials are functional in electrochemistry having a high surface-to-volume ratio [21].

The sinking compact diameter of layered 2D materials would result in reduced volume, trimmed mass, and eventually the low cost of several devices in many different fields. Layered 2D materials have numerous applications in various domains based on their optoelectric character like in solar cells, photonics, protective light-absorbing layers, spintronics, conductive displays, and valleytronics, etc. [22,23]. As, vigorous attention has been paid to graphene from last many years and many review articles are available in literature so here we directly jump to layered TMDCs in this review article, detailing MoS_2 and its incorporation in solar cell devices.

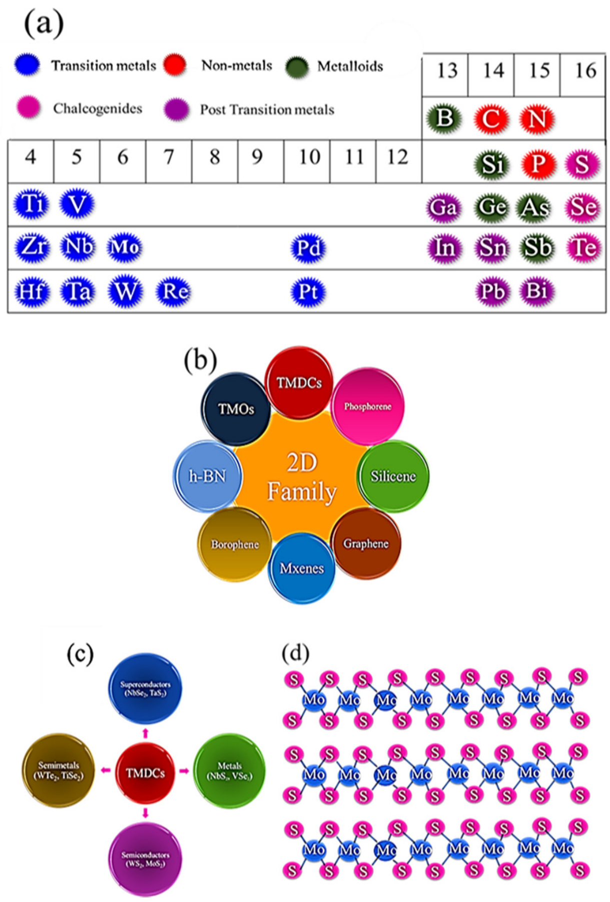

Figure 2. The house of the 2D family. (**a**) The spotlighted elements of the periodic table form's most popular two-dimensional layered materials. (**b**,**c**) Classification of the 2D material's family and the family of Transition Metal Dichalcogenides (TMDCs), respectively. (**d**) Layered structure of MoS_2 following the generic formula of MX_2 in TMDCs.

2. Transition Metal Dichalcogenides (TMDCs)

Layered 2D transition metal dichalcogenides contain a prodigious number of crystals and are represented by the general formula of MX_2 where M is a transition metal from groups IV B, V B, VI B, VII B (Ti, Zr, Hf, V, Nb, Ta, Mo, W, Tc, Re) and X is a chalcogen element from group VI A (S, Se, Te) [4,24,25]. Figure 2b shows the general classification of 2D family. Depending upon the layer number, elemental conjunction, and presence or absence of dopant, TMDs exhibit a bandgap ranging from 0 to 2 eV, unlike the pure graphene which is a semimetal with 0 eV bandgap [21,23,26].

Transition Metal Dichalcogenides (TMDCs) are metals, semimetals, semiconductors, insulators, and superconductors conditioning on the elemental composition and structural layout as shown in Figure 2c. Layered TMDCs are leading successors of graphene and they are transparent, flexible, and as thin as graphene [27]. Apart from sharing comparability of bandgap, on/off ratio, and charge carrier mobility to that of ever-present silicon, TMDCs can also be stacked on to the flexible substrate and can bear stress and strain consents of flexible supports [28,29]. Among TMDCs, in this presented review, the ruling material is MoS_2 because of its popularity based on the captivating properties.

Crystalline Structure of MoS_2

In each layer of TMDCs (MX_2) [30], the atomic layer of transition metal (M) is sandwiched between two atomic layers of chalcogens (X) as depicted in Figure 2d. In an MX_2 monolayer, a covalent bond is formed by coordination of d orbital of M and p orbital of X atoms. Every individual layer is clenched by delicate Van der Waals forces. Considerably, all the approachable orbitals are tangled in intralayer bonding, in this scenario, only the high energy anti-bonding orbitals would be left behind for inter-layer bonding, accompanied with the absence of dandling bonds [31]. Because of weak Van der Waals forces between each layer, bulk TMDCs can be exfoliated into monolayers by chemical, mechanical, or electrochemical exfoliation methods. On account of the quantum confinement effect and surface properties, there are various properties observed in monolayer TMDCs which are not observed in their bulk counterparts. Layer dependent properties change when the thickness is being changed. The bandgap of TMDCs converts from indirect to direct: For example monolayer TMDCs, like MoS_2 (1.8 eV), $MoSe_2$ (1.5 eV), (2H)-$MoTe_2$ (1.1 eV), WS_2 (2.1 eV), and WSe_2 (1.7 eV), display direct bandgap, though their bulk counterparts show indirect bandgap accompanying smaller energies [26,32].

MoX_2 can formulate three types of crystal structures based upon the atomic stacking geography, trigonal prismatic (2H) phase, an octahedral (1T) phase, and rhombohedral (3R) phase [33,34]. In the 2H MoX_2 phase, every Mo atom prismatically collaborates to six neighboring S atoms and in the 1T-MoX_2 phase, the nearby six S atoms exhibit a distorted octahedron, circling one Mo atom. The 2H phase is thermodynamically stable and the 1T phase is metastable. The more inspiring thing is the interconversion of these two phases by intralayer atomic drift. According to these conditions by Li and K intercalation, 2H-MoS_2 can be transformed into the 1T-MoS_2 phase [35]. Therefore, the IT-MoS_2 phase is thermodynamically unstable, it converts back to the stable trigonal prismatic 2H-MoS_2 phase at room temperature. Both of these phases reveal contrasting electronic effects like the 1T-MoS_2 phase shows metallic [36] properties, whereas the 2H-MoS_2 phase represents semiconducting behavior and 1T-MoS_2 phase seems to be a more zestful catalyst for hydrogen evolution as compared to 2H-MoS_2 semiconducting phase. The 1T-MoS_2 phase shows metallic properties, whereas the 2H-MoS_2 phase represents semiconducting behavior which is important for optoelectronic devices [37].

Raman spectroscopy comfortably spots 1T and 2H phases. The A_{1g} and E_{2g} vibrational modes of the 1T-MoS_2 phase and 2H-MoS_2 phase have shown at ~380 and ~410, respectively. The 1T-MoS_2 phase displays several vibrational modes, because of their symmetric dissimilarities, classified as j_1 (~160 cm^{-1}), j_2 (~230 cm^{-1}), and j_3 (~330 cm^{-1}); no such vibrational modes were observed in case of 2H-MoS_2 phase [38,39]. It is not facile to acquire exact quantitative scrutiny of phase format from Raman spectroscopy singly because of the feeble Raman response of these vibrational modes. X-ray photoelectron spectroscopy (XPS) is an auxiliary technique to provide a significant quantitative analysis of 1T and 2H-MoS_2 phases. For pure 1T-MoS_2, the Mo 3d zone exhibits peaks at ~228.1 eV and at ~231.1 eV which are slightly at lower binding energies than those disclosed for the pure 2H-MoS_2 phase (~229.5 and ~232.0 eV) [40]. Raman spectroscopy is also helpful for locating the number of layers in TMDCs [41,42].

Numerous electronic properties of TMDCs emerge by stuffing the non-bonding d-bands, exhibiting metallic behavior when the orbitals are partially inhabited, and they show semiconducting properties when the orbitals are completely filled [43]. Chalcogen atoms have a slight impact on the electronic structure as compared to that of metal atoms, still, it is noticed that the bandgap decreases due to the broadening of d-bands by raising the atomic number of chalcogen atoms [44].

3. Synthesis of Two-Dimensional Materials

Two-dimensional materials are elucidated as a set of untied layered nanosheets, disclosing an elevated ratio of lateral size (from tens of nanometers to tens of microns) to thickness (from a few angstroms to a few nanometers) [11]. Graphene, exhibiting a single carbon layer of the honeycomb-like lattice structure, is the most popular and papery 2D material [45]. Depending upon the anatomy and crystallographic configurations, 2D materials are synthesized in the past decennary [46,47]. There is no uncertainty that two-dimensional materials have captivated researchers and engineers in various fields due to the fact of their gigantic number of species, considerably their distinctive properties and their auspicious applications in several fields like optoelectronics, energy conversion, energy storage, and electronics, etc.

There are a number of methods for synthesis of 2D materials, as listed in Figure 3a, including: Hummer's method [48], micromechanical cleavage [1,49,50], liquid exfoliation [51] assisted by ion intercalation [52–55] and mechanical force [47,56–59], oxidation assisted liquid exfoliation [17,49,60], chemical vapor deposition [61–65], wet chemical synthesis method [66–69], electrochemical exfoliation [70–74], ball milling [51,75], etching-assisted exfoliation etc. [76–78]. All these methods can be grouped in two major classes of top-down and bottom-up approaches.

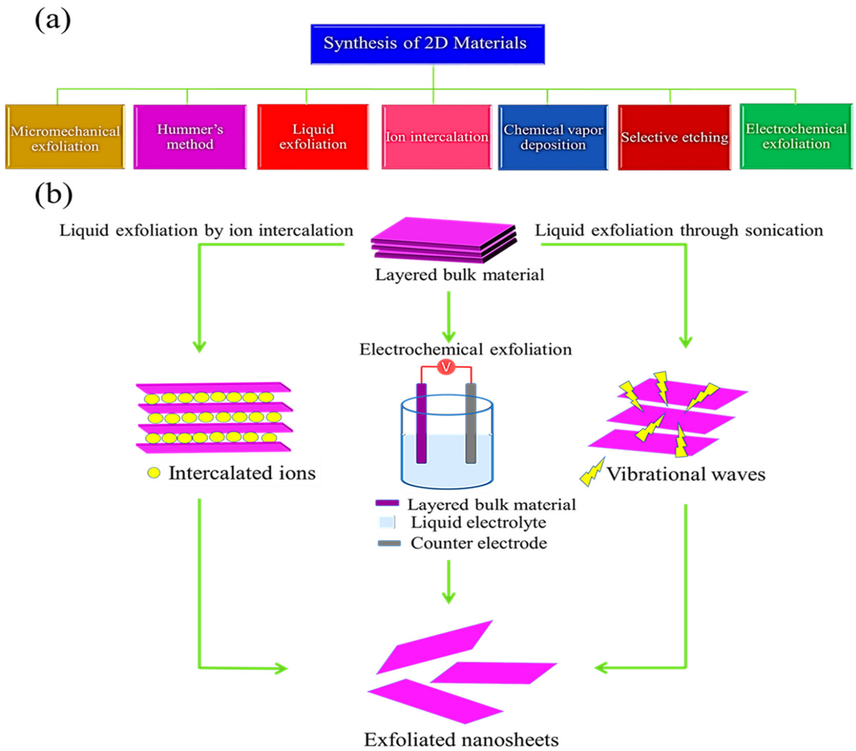

Figure 3. (**a**) Classification of synthetic strategies for 2D materials. (**b**) A simplified schematic of the liquid phase and electrochemical exfoliation of layered bulk material into 2D nanosheets.

In contrast to the bottom-up approach, top-down synthetic methods exhibit appreciable superiorities. Top-down synthesis methods give scalable production of exfoliated two-dimensional materials in an inexpensive and uncomplicated manner due to the low priced and highly available layered precursor material. The top-down approach includes synthetic methods such as liquid exfoliation through ion intercalation and mechanical force, liquid exfoliation through oxidation, and etching-assisted exfoliation, etc. Top-down approach is only limited to the 2D materials, of which the parental bulk counterpart is a layered material; however, the bottom-up approach is somehow more versatile in principle. Besides, downsides of top-down approach are also there such as defects production, more time consumption, and utilization of high-risk chemicals. Chemical vapor deposition (CVD) and epitaxial growth include the chemical reaction of precursors at specified experimental conditions.

The bottom-up synthesis method is nearly applicable to the exfoliation of all types of ultrathin 2D materials. Both, CVD and epitaxial growth processes take place at high temperature and vacuum. Moreover, an extra transfer step is required to shift the products from the metal surface to the selected substrate. During the transfer process, the risk of impurities enhances and it costs much higher.

Until now, a tremendous bloodline of 2D materials has been recorded such as transition metal dichalcogenides (TMDCs), graphene, graphitic carbon nitride (g-C_3N_4), black phosphorene, graphene oxide (GO), reduced GO (rGO), hexagonal boron nitride (h-BN), oxides, MXene, etc. Superb qualities have been shown by TMDCs (e.g., Ta_2NiS_5, WS_2, Bi_2Te_3, $NbSe_2$, VSe_2, Sb_2Se_3, WSe_2, MoS_2, and Ta_2NiSe_5) other than graphene. Alongside graphene, MoS_2, has come to the light as a future candidate for optoelectronic applications, exhibiting excellent performance due to the face of its direct bandgap, quantum confinement, and higher mobility. Now, researchers are more interested in other 2D materials to enhance properties, like MoS_2 and h-BN, beyond graphene to compensate for the drawbacks of graphene. Because of zero bandgap, graphene has lost its application in optoelectronic devices and field-effect transistors. In this article, we will discuss the most common synthesis methods of MoS_2, WS_2, and graphene.

3.1. Synthetic Strategies for Graphene: Graphene as a Beginner

Here, we discuss the synthesis of the very first 2D materials which further extend to other 2Ds. Graphene is almost 1×10^6 times more slimmer than a human hair and approximately two-hundred-fold more powerful than steel. Additionally, graphene [79] is a better conductor than copper. There are numerous methods for the synthesis of 2D materials [7,46,80–83]; most commonly, one of them is the micromechanical cleavage method [1,50,51]. Energy is required to exfoliate the layered material into nanosheets [50,84]. In this prevailing cleavage method, Scotch tape is used for exfoliating the layered bulk crystals into nanosheets. [85] The intention to apply the mechanical force through Scotch tape is to weaken the out of plane Van der Waals forces without shattering the in-plane strong covalent bonds within each layer, consequently taking off a single or few layers of 2D materials. In the conventional method, the bulk 2D material (e.g., graphite) is attached to the sticky part of the Scotch tape and then take it off into single or few layers by adhering it to another sticky surface [1,51]. This process is replicated again and again in order to obtain the suitable thickness of flakes. Then, in the transfer method, split flakes on the Scotch tape are attached to the suitable substrate and peeled off from Scotch tape, leaving behind a single or few layer nanosheets on the substrate [50].

First, Novoselov, Geim, and co-workers [1], in 2004, mechanically exfoliated graphite into graphene nanosheets [86,87] and received a Noble Prize in 2010 [88]. Later on, this technique was also being used for the exfoliation of other 2D materials particularly the TMDCs, e.g., TiS_2, $MoTe_2$, $TaSe_2$, $MoSe_2$, WS_2, TaS_2, WSe_2, ReS_2 [50,88], h-BN [1,89], and metal phosphorous trichalcogenides, etc. There are numerous benefits of micromechanical cleavage method worth nothing, such as its harmlessness, because there is no use of chemicals; ideal crystal grade; and clean and defect-free surfaces with large lateral sizes [90]. Despite all these advantages, some flaws hamper its practical applications. First, mass production is not possible. Second, the yield is low compared to solution-based synthesis techniques. Thirdly, there is no control over the size, thickness, and morphology of nanosheets. Because the entire process is carried out manually, this is why there is deprivation of precision and repeatability [91].

3.1.1. Liquid Exfoliation of Graphene

For the exfoliation of graphite into graphite oxide, there is an additional extensively used method, which is called liquid exfoliation, assisted by oxidation [60]. Benjamin Collins Brodie [92], a British chemist, is known to be the first researcher who disclosed the fascinating properties of graphite oxide in 1859 [92]. From then on, because of the captivating properties of graphene oxide (e.g., super strong, highly conductive, thinness, and its wide applicability in various fields), GO appeared as one of the famous 2D materials and welcomed by the researchers. According to Brodie's method, a mixture of graphite and potassium chlorate ($KClO_3$), with the ratio of 1:3, was reacted with fuming HNO_3 for 3 to 4 days at 60 °C. Staundenmaier [93] in 1898, upgraded Brodie's work by replacing fuming HNO_3 with H_2SO_4 and used manifold $KClO_3$ [93]. But this method caused hazards because of the usage of $KClO_3$, which is the source of the persistent explosion, and also it is a time taking reaction that takes 4 days [94]. Then, Hofmann in 1937, almost after 40 years, used non-fuming HNO_3 for the synthesis of graphene instead of fuming HNO_3 and revealed one more novel method that is more applicable and uncomplicated because of no requirements of repetition of oxidation process by four times [95,96].

In 1958, the chemist Hummer and his coworkers [48] developed a method for the synthesis of graphene oxide, this method is still used extensively [48], called Hummer's method. In Hummer's method, $KClO_3$, being replaced by $KMnO_4$ to prevent continuous explosion and $NaNO_3$ replaced fuming HNO_3 to prevent the production of fog acid. The fundamental principle behind this method is the utilization of an extremely powerful oxidizing agent to make sure the oxidation of graphite into graphite oxide. Frequently applied oxidizing agents are $KMnO_4$ and concentrated H_2SO_4 [17] due to the vigorous oxidizing power of ions such as SO_4^{-2} and MnO_4^{-2}. Nitric acid is an exemplary intercalation representative, which expands the interlayer spaces and, thus, assists the intercalation of oxidative agents into the host galleries.

Some additional oxidative agents also cause the exfoliation of graphite, following the same mechanism of exfoliation, afar from ordinary ones [97]. On the surface of each graphene layer, functional groups containing oxygen species are developed due to the oxidation of graphite, which can cause the outstanding expansion of interlayer spacing of the bulk crystal and consequently remarkably debilitate the Van der Waals forces between the adjoining layers [49–61]. With the successive sonication remedy, single-layer graphene nanosheets are produced by the exfoliation of expanded graphite oxide. This method is useful for the production of graphene oxide nanosheets [49,61,62]; however, it cannot be applied further for exfoliation of other 2D materials. Hummers' method is good in the way to give the mass production of GO nanosheets in solution with a major disadvantage of using a powerful oxidizing agent. This method is not as safe as the sonication assisted liquid exfoliation method. Hummer's method fabricates more oxygen quantity than Brodie's method [98]. But still, there are some flaws in hummer's method [99] i.e., the production of toxic gases like NO_2 and N_2O_4 [95]. Marcano et al. [100] distinguished hummer's method, modified hummer's method [101,102], and improved hummer's method for the synthesis of graphene nanosheets based on the degree of oxidation of end product [100,103–106].

Epoxy, carboxyl, and hydroxyl, oxygen-containing functional groups are being introduced on the surface of graphene oxide due to the oxidation [107]. The oxygen-containing functional groups can be partially eradicated from the surface by reduction of the oxygen-containing specie, graphene oxide, into reduced graphene oxide (rGO) nanosheets. There are numerous approaches for the reduction of GO nanosheets (e.g., reduction through chemical reaction by using reducing agents), photochemical reduction, reduction by electrochemical means, thermal annealing, and others [61,74,104,108–113]. GO as well as the rGO, show different electronic, physical and chemical properties in contrast to their bulk counterpart (pristine graphene). The most striking distinction is the superb electrical conductivity of graphene, while GO nanosheets are electrically insulator [114]. Even though, GO nanosheets reduced back to the rGO nanosheets, but the electrical conductivity was not comparable to the graphene obtained from CVD method or through mechanical exfoliation method. Furthermore, GO has functional groups on its surface, it is hydrophilic and admirably dispersible in water [115], whereas on the other side, graphene is hydrophobic [116]. Due to these distinguishing characteristics, GO and rGO are called derivatives of graphene, rather than just saying them, graphene. The electrical conductivity can be manipulated, to electrical conductor from insulator, by precisely adjusting the number of oxygen-containing functional groups on the surface of GO [107].

3.1.2. Electrochemical Exfoliation of Graphene

By moving forward from Scotch tape cleavage and liquid exfoliation method, electrochemical exfoliation is another method for exfoliation of graphite into its 2D morphology. The utilization of the suggested by Brodie, Staudenmaier, and Hummers is well known for mass production and low cost. However, these methods involve strong oxidants and acids which results in the emission of toxic gases and can also deteriorate the sp^2 bonding in graphene. Moreover, these methods are time-consuming including the production of defects as well. Most recently, considerable attention has been paid to the electrochemical exfoliation method for the synthesis of graphene nanosheets. Electrochemical exfoliation is simple, greener, fast, scalable, and low-cost synthesis method and gives a product (graphene) with lesser defects and higher crystallinity. This method also allows the tuning of the degree of oxidation in the product. Table 1 briefly describes the efforts of different research groups for the synthesis of graphene nanosheets by the method of electrochemical exfoliation of graphite.

Table 1. Strategies to synthesize graphene using a series of electrochemical exfoliation methods.

Synthesis Strategy	Title of Paper	Specifications	Year of Publication	Author + Reference
Electrochemical exfoliation	One-step ionic-liquid-assisted electrochemical synthesis of ionic-liquid-functionalized graphene sheets directly from graphite	1-octyl-3-methyl-imidazolium hexafluoro-phosphate (8mim + PF6) (ionic liquid IL) along with water used as an electrolyte. Two graphite rods were used as electrodes. Obtained graphene nanosheets (GNs) did not disperse in water but polar aprotic solvents.	2008	B.N. Liu et al. [117]
Electrochemical exfoliation	One-pot synthesis of fluorescent carbon nano-ribbons, nano-particles, and graphene by the ex-foliation of graphite in ionic liquids	Synthesis of graphene sheets in a single vessel using graphite rod and platinum wire as electrodes and 1-methyl-3-butylimidazolium tetrafluoro-borate (or 1-methyl-3-butylimidazolium chloride) as an electrolyte in combination with water in varying ratios.	2009	Lu et al. [118]
Electrochemical exfoliation	An electro-chemical route to graphene oxide	Expanded graphite used as anode and Pt wire as a counter electrode along with KCl as an electrolyte. 1.9, 2.8, and 3.9 nm were the thicknesses of mono, bi, and tri-layers of graphene, respectively.	2011	You et al. [119]
Electrochemical exfoliation	High-quality thin graphene films from fast electrochemical exfoliation	Highly oriented pyrolytic graphite (HOPG) used as a graphene source, grounded Pt wire used as a counter electrode, and H_2SO_4 used as the electrolyte. The lateral size of the exfoliated graphene sheet was 30 µm. The transparent conducting film, containing these exfoliated graphene sheets, was good in conductivity but the yield was low.	2011	Su et al. [120]
Electrochemical exfoliation	Synthesis of high-quality graphene through electro-chemical exfoliation of graphite in alkaline electrolyte	Graphite rod and platinum wire were used as electrodes along with alkaline electrolyte (KOH) in the electrochemical setup. Graphene is obtained with fewer defects, good quality, 1–4 layers, and with lateral size up to ~80 µm.	2013	Tripathi et al. [121]
Electrochemical exfoliation	Electrochemically exfoliated graphene as solution-processable, highly conductive electrodes for organic electronics	H_2SO_4, graphite flakes, and platinum wire were used as electrolyte, anode, and cathode respectively. The thickness of graphene flakes was ~1.5 nm for bilayer and size of exfoliated graphene sheets was up to 5–10 µm.	2013	Parvez et al. [122]
Electrochemical exfoliation	Few-layer graphene obtained by electrochemical exfoliation of graphite cathode	A system of dimethyl sulfoxide (DMSO), NaCl, water, and thionin acetate was used as an electrolyte for exfoliation of graphite cathode. Acquired graphene sheets contained less degree of oxidation as well as defect sites.	2013	Zhou et al. [123]
Electrochemical exfoliation	Synthesis of graphene oxide nano-sheets by electrochemical exfoliation of graphite in cetyl-trimethylammonium bromide and its application for oxygen reduction	Cetyltrimethylammonium bromide (CTAB) used as electrolyte where-as graphite rod and Pt wire was used as electrodes. GO/CTAB suspension is tremendously stable in ambient conditions. The single-layer thickness of the obtained graphene is 2.5–4.5 nm.	2014	Kakaei and Hasanpour [124]
Electrochemical exfoliation	Role of peroxide ions in formation of graphene nanosheets by electrochemical exfoliation of graphite	A network of $NaOH/H_2O_2/H_2O$ was used to exfoliate graphite. High-quality graphene sheets with 3–6 layers are formed exhibiting a thickness of ~1–2 nm with a 95% yield.	2014	Rao et al. [125]
Electrochemical exfoliation	Exfoliation of graphite into graphene in aqueous solutions of inorganic salts	Inorganic salts such as $(NH_4)_2SO_4$, K_2SO_4, and Na_2SO_4 used as electrolytes for the synthesis of graphene sheets. Graphene sheets showed vast lateral size, low oxidation level, and elevated yield of 85%.	2014	Parvez et al. [53]
Electrochemical exfoliation	Graphene synthesis via electrochemical exfoliation of graphite nanoplatelets in aqueous sulfuric acid	Utilized pressed-graphene nanoparticles (GNP) used as anode and Pt wire as a cathode with 0.1M sulphuric acid as an electrolyte. Flakes size is more manageable	2016	Lin Li et al. [82]
Electrochemical exfoliation	Preparation of graphene sheets by electrochemical exfoliation of graphite in confined space and their application in transparent conductive films	In EECS (electrochemical exfoliation in confined space) nickel foam is used as a counter electrode while the working electrode is graphite rod covered with paraffin, with bottom opening, in an alkaline electrolyte (10 mol/L NaOH). Paraffin helps to control the extravagant exfoliation of graphene. Graphene rooted conductive sheets can replace indium tin oxide.	2017	Hui Wang et al. [126]

Table 1. *Cont.*

Synthesis Strategy	Title of Paper	Specifications	Year of Publication	Author + Reference
Electrochemical exfoliation	Electrochemical exfoliation synthesis of graphene	Graphite rod and Pt wire placed vertically in the electrochemical cell along with protonic acid as an electrolyte. In the vertical configuration, exfoliation is much better organized and graphene synthesized with better quality as well as quantity.	2017	J. Liu and Theses [127]
Electrochemical exfoliation	Electrochemical exfoliation of graphite into graphene for flexible supercapacitor application	Graphite rod and Pt used as electrodes, 0.1M potassium sulfate used as the electrolyte. The size of graphene nanosheets is in between of 433 nm to 5.07 µm.	2018	Singh and Tripathi. [128]
Electrochemical Exfoliation	A facile synthesis of graphene oxide (GO) and reduced graphene oxide (rGO) by electro-chemical exfoliation of battery electrode	GO being synthesized by using ionic specie as an electrolyte, graphite rods as electrodes, and regulated DC power supply. GO being reduced to rGO using ascorbic acid, i.e., environment-tally benign reducing agent.	2019	Vartak et al. [129]
Electrochemical exfoliation	Controlled synthesis of graphene via electrochemical route and its use as efficient metal-free catalyst for oxygen reduction	$(NH_4)_2SO_4$ used as electrolyte whereas Pt and graphite substrate served as the two electrodes in electrochemical setup. High standard graphene with governable layer number was fabricated using cost-effective precursors.	2019	Komba et al. [130]
Electrochemical exfoliation	A single-step strategy to fabricate graphene fibers via electrochemical exfoliation for micro-super capacitor applications	The simplistic, economical top-down synthesis method is used to fabricate porous, fiber-like graphene. Graphene fibers showed high specific capacitance, high electrochemical performance because of porous structure and fine electronic conductivity.	2019	He et al. [131]

3.2. Synthetic Strategies for TMDCs

In 2004, after the successful exfoliation of graphene from graphite, by Novoselov and his coworkers [1], a series of experiments were performed on TMDCs, more specifically on MoS_2 [132]. Nevertheless, TMDCs traveled the journey of seven years to step out of the umbra of famous graphene to certify their identification. To formulate their various 2D forms, a variety of exfoliation methods has been originated to split the piled-up layers in bulk TMDCs [133–135]. The basic drive behind the exfoliation of liquids is to provide a suitable amount of energy to the liquids to conquer the van der Waals interactions between the layers. Synthesis methods including micromechanical cleavage, liquid exfoliation, intercalation, etc., are classified under top-down synthesis methods. Top-down and bottom-up approaches have been discussed in Section 3.

The strong in-plane bonding and relatively delicate interlayer bonding enables the layered 2D materials to be separated into isolated, atomically slim nanosheets, where nano adverts to the extent of thickness [57]. Micromechanical cleavage [49,50], discussed in Section 3.1, is the foremost successful method to spare 2D layered materials into the individual layers from their bulk counterparts [88,136]. No doubt, the micromechanical cleavage method [49] gives fine quality mono and few layers with the least defects, but this method is restricted due to low yield and deficient thickness control. To overcome this problem, one popular method is the liquid phase exfoliation through the solvent, sonication, and with/without ion intercalation strategy.

3.2.1. Liquid Phase Exfoliation of TMDCs

Liquid phase exfoliation is the most extensively applied synthesis method to fabricate the nanosheets of TMDCs [137–139]. The basic mechanism behind liquid exfoliation involves three steps. Firstly, the dissolution of the respective bulk TMDCs in the suitable solvent. Secondly, the exfoliation of the bulk counterpart into nanosheets by sonication. However, surfactants are added as a stabilizing agent [140,141]. Third and the least one, separation of individual sheets and centrifugation. Figure 3b is the simple schematic demonstration of liquid phase exfoliation through sonication and ion intercalation and exfoliation through the electrochemical method to obtain the nanosheets at the end as a major product. A wide domain of other 2D materials can also be synthesized such as graphene [142–145], boron nitride [146,147] and phosphorene [148,149] by this method. Depending on the energy source implemented for exfoliation and dispersion of nanosheets, the liquid phase exfoliation method has been divided into two categories, i.e., liquid exfoliation through sonication [150] and liquid exfoliation through sheer force.

In the liquid phase, bulk TMDCs can be converted into nanosheets by sonication [151,152]. Following the dispersion of bulk powder in the required solvent (e.g., *N*-methyl-2-pyrrolidone, NMP) for exfoliation, a probe sonicator, a bath sonicator or the combination of both of them, is used. In ultrasonicated dispersions, because of cavitation bubbles' collapse, microjets and shock waves are produced [153–155], which causes the exfoliation of bulk crystal into nanosheets in the liquid phase [156]. To get the systemized exfoliation of TMDs, the critical aspect is the comparable surface energies of bulk TMDs crystal and the solvent being used. The dispersion, after sonication, treated with centrifugation for about an hour at 500–1500 rpm [157]. Ultimately, the supernatant, containing mono and few-layer nanosheets of MX_2, collected from centrifuged dispersion. This obtained dispersion of nanosheets is suitable for a number of techniques such as electrodeposition, spray coating, spin coating, vacuum filtration, etc. [158,159].

From all around the world, there are a large number of research groups, including the Ajayan group [86] and Coleman group [159], they applied liquid phase exfoliation in different liquid media and synthesized almost all 2D materials [86,156,157]. In a guideline article, the method of exfoliation, characterization, and processing of 2D materials has been discussed by Backes, Coleman, and coworkers [160]. Additionally, they facilitated the research world with a tutorial video as well [161]. Liquid phase exfoliation through sonication has an energetic group with wealthy literature and in recent years the discipline has been massively reviewed.

Via a range of experiments, Coleman et al. [157] proposed the optimized solvents for MoS_2 and WS_2. Different 2D materials have different surface energies, and consequently, different solvents are required to form the stable dispersions of different materials [162,163]. Precisely, the surface energies of MoS_2, h-BN, and graphene are 46–65 mJ cm^{-2}, 44–66 mJ cm^{-2}, and 70 mJ cm^{-2} [157,164]. Many good solvents like NMP and DMF (*N*,*N*-dimethylformamide) have high boiling points and the leftover solvent can damage the 2D materials. That's why, the solvents having low boiling points would be preferred [165,166]. There is a vast collection of solvents in literature (e.g., 1-butyl-3-methylimidazolium chloride ionic, tetrahydrofuran (THF), methanol, acetone, and ethanol, etc.), to make nanosheet's dispersions of MoS_2 [167]. For exfoliation of transition metal dichalcogenides by sonication in water or the solvents having low boiling points, a diversity of ionic surfactants [168], polymers [169–171], and nonionic surfactants [172,173] have been practiced in literature.

Although, an appreciable amount of 2D materials can be achieved through sonication assisted liquid exfoliation as compared to micromechanical cleavage method, still, this method cannot cover the requirements for industrial exertion. To boost up the mass production of 2D materials, the exfoliation of 2D materials was supported by shear force in liquid media [174,175]. A method raised by Paton et al. [176], shear force assisted exfoliation in the liquid phase, applying shear force for exfoliation of 2D materials accompanied by intense shear rates. Coleman and his coworkers [176], implemented a rotor-stator mixer with a high shear rate to promote the production rate of graphene thin flakes [176]. In the liquid, carrying the bulk 2D crystal, a mixer can kindle the intense shear rates under strong rotation speed [50]. The shear forces under the influence of intense shear rates prompted the exfoliation of bulk 2D materials in the liquid phase. The utilization of suitable solvents and polymers can prune the energy tariff of the exfoliation method as well as provide the stability to nanosheets. This method further implemented for the exfoliation of graphene, h-BN, and TMDs [177,178].

Exfoliation through ion intercalation in liquid media is an additional example of the top-down synthesis method. The core objective of this method is to inject the cation ions (e.g., Cu^{2+}, Na^+, K^+, or Li^+ ions), in the host material galleries, having a small ionic radius to form the ion-expanded compound. Conventionally, reducing agents and electron donor species could be injected directly in between the layers of bulk 2D materials [179]. Ion intercalation causes the expansion of the layers in host 2D material and deliberate the van der Waals interlinkages between the adjoining layers in the bulk material [122,180]. The ion injected compound can be comfortably exfoliated into mono or few layers nanosheets under specific conditions, i.e., specific solvent, sonication time, etc. For the above half-century almost, intercalation of alkali metal ions have been investigated [181]. The key benefit of alkali metals is their smaller size, which helps to get into the host galleries. The addition of alkali metal-expanded layered material into water causes the hydrogen bubble formation in the liquid, which causes further expansion of layers and helps exfoliation of the bulk crystal. The most frequently used alkali metal is Li, using organometallic compounds (e.g., *n*-butyllithium) for intercalation, which possesses the smallest size and exhibits higher reactivity as compared to the other alkali metals. A large number of layered materials can be exfoliated using Li^+ intercalation, e.g., graphene, h-BN, TMDCs, etc. [35].

Back to the 1980s, Morrison, and co-workers [182] exfoliated bulk MoS_2 crystal into monolayered MoS_2 nanosheets, using n-butyllithium being intercalator, by Li intercalation method in liquid media. Large compounds, like *n*-butyllithium (*n*-BuLi) including *tert*-butyllithium (*t*-BuLi) exhibit more effective exfoliation as compared to smaller compounds such as methyllithium (MeLi) [183,184]. In the conventional process, 2D bulk materials, in the environment of Ar or N_2, introduced into the n-butyllithium solution for some days. High temperature or stirring is being frequently used to enhance the efficiency of the intercalation process. By injecting lithium ions (Li^+) between the layers, exfoliation of Li_xMoS_2 takes place, through hydrolysis, into monolayers. At the hydrolysis stage, ultrasonication being applied to enhance the hydroxyl group diffusion and to improve the exfoliation efficiency [185]. Eda et al. [186] used *n*-BuLi to exfoliate MoS_2 with 50% semiconducting 2H-MoS_2 phase and 50% metallic 1T MoS_2 phase. Zheng et al. [54] used the ion intercalation process in combination with the hydrothermal method to synthesize the large area MoS_2 nanosheets [54]. Other than *n*-butyllithium, some other compounds ($LiBH_4$) also proved efficient intercalators for 2D nanomaterials [187]. Pumera and coworkers [188] compared Li intercalation process efficiency and transitions between 1T and 2H phases of $MoSe_2$, MoS_2, WSe_2, and WS_2. Moreover, with the help of ultrasonication [189] and microwave-induced intercalation [190], the efficiency of the Li intercalation process can be improved. Liquid exfoliation through the ion intercalation process has been applied to synthesize various 2D nanomaterials like Cu_2WS_4, $MoSe_2$, WS_2, MoS_2, ReS_2, and TiS_2 [54,191,192].

Limitations to the Li intercalation process are there as well. Usage of organometallic compounds, which are reactive to air and moisture and are explosive, N_2 or Ar glove box is required. Additionally, long reaction time, insufficient monolayer yield, deprivation of semiconducting phase, the inadequacy of controllability, and lateral sizes of exfoliated sheets are in the sub-micron region, are drawbacks of Li intercalation process [184,193]. Consequently, some intercalators, other than lithium, being used by scientists to improve the exfoliation efficiency of TMDCs [55,194–196].

3.2.2. Electrochemical Exfoliation of MoS_2/WS_2

To produce the solution-processable and large scale exfoliated MoS_2 by chemical means [197–199], enormous attempts have been committed. Among those attempts, the electrochemical exfoliation method is one. The utilization of the electrochemical approach assists the exfoliation process for the mass production of two-dimensional layered materials. Table 2 compiles the research efforts from 2010 to 2018 in the electrochemical exfoliation of MoS_2 from bulk to its nanosheets. Zeng et al. [199] used MoS_2 bulk material as cathode and lithium foil as a counter electrode in the electrochemical setup. Lithium ions get incorporated between the layers and cause exfoliation. In the course of intercalation of lithium ions, every Li atom also inserts one electron with it in host layered material. The intercalation of a large number of lithium ions causes massive injection of electrons in MoS_2 layered material (host material) which gives rise to the undesired transition of the 2H-semiconducting phase into 1T-metallic phase. You et al. [200] exfoliated MoS_2 by using H_2SO_4 as electrolyte and platinum as a counter electrode. Later, the aforementioned group modified the exfoliation method by incorporating SO_4^{-2} ions at neutral pH value and resulted in the generation of MoS_2 nanosheets with large lateral size and having a lower oxidation level as well [201]. There are various constraints and challenges, in the electrochemical exfoliation method, which have to be taken into consideration while talking about two-dimensional materials except for graphene. Major restriction is the need of conductive material, so the method is restricted to only conductors and semiconductor materials. Moreover, there are some other parameters of study like material should be strong enough to resist the chemical changes due to anodic or cathodic oxidation and should have stability in ambient circumstances as well. Only MoS_2, Bi_2Se_3, graphene, black phosphorous, and Bi_2Te_3 have been successfully exfoliated in aqueous electrolyte by electrochemical means because this method is in premature stage for 2D materials other than graphene and a lot of work must be done in this area [202].

Table 2. Electrochemical exfoliation methods for the synthesis of MoS_2/WS_2 nanosheets.

Synthesis Strategy	Title of Paper	Specifications	Year of Publication	Author + Reference
Electrochemical exfoliation	Single-layer semiconducting nanosheets: high-yield preparation and device fabrication	The multi-layered bulk material (MoS_2, WS_2, Graphene, etc.) was used as a cathode in the electrochemical cell while lithium foil being used as an anode. $LiPF_6$ used as an electrolyte. Monolayer yield is 92% in this method for MoS_2.	2011	Zeng et al. [199]
Electrochemical exfoliation	Large-area atomically thin mos2 nanosheets prepared using electrochemical exfoliation	Na_2SO_4 being used as an electrolyte along with a pure single crystal of MoS_2 as a working electrode and Pt wire as a counter electrode. This synthesis method ended up giving the yield of MoS_2 monolayers up to 5–9% with 50 µm lateral size of sheets, little oxidation and acceptable quality.	2014	Liu et al. [201]
Electrochemical exfoliation	Electrochemical exfoliation of mos2 electrogeneration crystal for hydrogen	Pt foil and MoS_2 crystal being used as electrodes in electrochemical setup including K_2SO_4 as the electrolyte. The obtained lateral size of MoS_2 nanosheets was 100–200 nm with 15–20 layers.	2018	Ambrosi & Pumera [71]
Electrochemical exfoliation	Solution-processable 2d semiconductors for high-performance large-area electronics	In electrochemical setup, MoS_2 crystal being intercalated by THAB (tetraheptylammonium bromide). After intercalation, the enlarged MoS_2 crystal was sonicated in PVP/DMF (poly-vinylpyrrolidone solution in dimethylformamide). PVP provided stability to the monolayers of MoS_2 from stacking back. Obtained nanosheets have had a thickness of 3.8 nm with a lateral size of 0.5–2 µm.	2018	Lin et al. [203]
Electrochemical exfoliation	Advanced composite 2d energy materials by simultaneous anodic and cathodic exfoliation	Single MoS_2 crystal sank in TBA^+ in electrochemical setup. Firstly, the bulk crystal was immersed in acetonitrile but later acetonitrile replaced by TBA^+ for better expansion. Cathodic exfoliation gave MoS_2 monolayers with great crystallinity and no defects were observed as well.	2018	Li et al. [204]

The sinking compact diameter of layered 2D materials would result in reduced volume, trimmed mass, and eventually the low cost of several devices in many different fields. Layered 2D materials have numerous applications in various domains based on their optoelectric character like in solar cells, photonics, protective light-absorbing layers, spintronics, conductive displays, and valleytronics, etc. [22,23]. As, vigorous attention has been paid to graphene from last many years and many review articles are available in literature so here we directly jump to layered TMDCs in this review article, detailing MoS_2 and its incorporation in solar cell devices.

4. Applications of MoS_2 in Opto-Electric Devices

Among 2D materials, graphene, a semimetal with zero bandgap, was the first to be tremendously used in various applications of science and technology [205]. However, due to the zero bandgap, graphene has restricted its applications in optoelectronics and field-effect transistors. In a very short time, following the disclosure of graphene, special attention was being paid to other 2D materials, e.g., h-BN, phosphorene and TMDCs, etc. [11,206]. Transition metal dichalcogenides (TMDCs) have diversity in terms of their properties like they exhibit excellent optical, mechanical, and electronic properties. As we are interested in optoelectronic properties for photovoltaic applications, the main focus is on optical and electronic properties [207]. In terms of optical properties, they give superb photoabsorption in visible and near IR range (absorption co-efficient is 10^5–10^6 cm^{-1}). Transition metal dichalcogenides (TMDCs) have a tunable bandgap, vary while reducing the thickness, show transition from indirect to direct bandgap, exhibit powerful light-matter interactions and due to the quantum confinement effect, they show intense photoluminescence. The direct bandgap, high mobility (50 cm^2/V s), and strong interaction with light give monolayer TMDCs a big breakthrough in applications of photovoltaics [208].

4.1. MoS_2 as Absorber Material in Solar Cells

Transition metal dichalcogenides (TMDCs), more specifically MoS_2, with a 2H crystal system, are largely acceptable in PV (photo voltaic) applications [209]. The bandgap of TMDCs varies from 1.0 to 2.0 eV, which is comparable with the solar spectrum, in correspondence with other famous solar cell semiconductors like Si (1.1 eV), CdTe (1.5 eV) and GaAs (1.4 eV) [210]. It has been stated that in the thickness of 1 nm, 2D TMDCs can show 5–10% absorption of incident light per unit volume and can attain higher absorption efficiency of sunlight, compared to the frequently used materials like Si and GaAs as light absorbers. The amount of light absorbed by the monolayer of TMDCs is comparable to the amount of light being absorbed by 50 nm thick Si layer and gives higher photocurrent values (2.0–4.5 mA/cm^2) [211].

4.2. MoS_2 as a Counter Electrode in Dye-Sensitized Solar Cells

In dye-sensitized solar cells, the counter electrode plays an important role by transferring electrons through an external circuit to tri-iodide ions for the reduction process. The photoelectrochemical process in DSSCs (Dye-Sensitized Solar Cells) strongly influenced by the electrocatalytic effect of the counter electrode [212]. MoS_2 is a replacement in DSSCs as a counter electrode as compared to traditionally used high-priced Pt electrode [213–215]. MoS_2 used in three contrasting structural architectures, i.e., MoS_2 nanoparticles, few-layered MoS_2, multi-layered MoS_2 as a counter electrode by Lei et al. [216]. The devices containing these MoS_2 morphologies exhibit the photon conversion efficiency of 2.92% for ML-MoS_2, 5.41% for MoS_2-NPs, 1.74% for FL-MoS_2.

MoS_2 implanted with graphene flakes also used as a counter electrode by Lin et al. [217] and power conversion efficiency (PCE) achieved was 6.07%. MoS_2 gives a fast reduction process of tri iodide ion and Graphene flakes, being highly conductive, give speedy charge transfer. Liu et al. [218] used nanocomposite of MoS_2/rGO as a counter electrode and reported PCE 6.04%.

4.3. MoS_2 as a Diverse Role Material in Organic Solar Cells

Organic solar cells have numerous remarkable properties in particular lightweight, flexibility, facile synthesis and solution processability, etc. In typical organic solar cell layout, a blend of photoactive material with electron donor and electron acceptor material is present. Mostly used hole transport layer is a blend of PEDOT: PSS (Poly (3,4-ethylenedioxythiophene): poly(styrene sulfonate) in organic solar cells. Graphene, TMDCs, and carbon nanotubes were investigated as a hole extraction layer in place of PEDOT: PSS blend [219].

MoS_2 can be used as a hole transport layer (HTL), electron transport layer (ETL), the buffer layer, and as an interfacial layer in organic solar cells [220].

Gu et al. [221] reported MoS_2 as a HTL instead of PEDOT:PSS in (poly({4,8-bis[(2-ethylhexyl)oxy]benzo-[1,2-b:4,5-b]dithiophene-2,6-diyl}{3-fluoro-2-[(2-ethylhexyl)-carbonyl] thieno [3,4-b]thiophenediyl}) PTB7: PC71BM based solar cell and also in (3-alkylthiophenes) P3HT: PC71BM ([6,6]-Phenyl C71 butyric acid methyl ester) based organic solar cells which exhibited PCE of 8.11% and 4.02%, respectively. In PTB7: PC71BM-based solar cells, PCE changes from 6.97% to 8.11% by changing the number of layers of MoS_2, showing the dependence of PCE on different number of layers of MoS_2. In PTB7: PC71BM-based monolayer MoS_2 solar cell, VOC of 0.69 V, fill factor of 64%, JSC of 15.78 mA/cm^2 and PCE of 6.97% obtained.

MoS_2 is also used as an anode buffer layer by Li et al. [222] in organic solar cells to prevent the current leakage between bare ITO and PC61BM and showed the PCE of 3.9%. PCE of 2.14% achieved in organic solar cells consisting of bare ITO without a buffer layer. A nanocomposite of PEDOT: PSS/MoS_2 can also be used as a hole extraction layer in P3HT: PCBM ([6,6]-phenyl-C61-butyric acid methyl ester) based organic solar cells giving PCE value of 3.74% [223]. Yang et al. [224] used MoS_2 as a hole withdrawing layer in the organic solar cell. In respective organic solar cell PTB7: PC71BM used as an active layer, PFN poly[(9,9-bis(3′-(*N*,*N*-dimethylamino)-propyl)-2,7-fluorene)-alt-2,7-(9,9−dioctylfluorene)] as the electron transport layer and oxygen-containing MoS_2 was used as hole withdrawal layer produced by UV–ozone treatment. As compared to PEDOT: PSS, both, MoS_2 nanosheets and oxygen containing MoS_2 nanosheets exhibited surpassing optical transparency in the region of 400–900 nm with PCE of 4.99%.

Hole transport material demands profound work function and there must be the material of low work function for electron extraction in organic solar cells, due to this reason, graphene and its derivatives can be used as both electron and hole extraction layers in the organic solar cell because of their tunability of work function. Yun et al. [225] used MoS_2 as an electron extraction layer and hole withdrawal layer as well. P-type doped MoS_2 used as a hole withdrawal layer and the n-type doped layer was used as an electron extraction layer. Photon conversion efficiency increased from 2.8% to 3.4% in organic solar cells containing p-type doped MoS_2 as a hole extraction layer.

MoS_2 used as an interfacial layer and silver nanowires along with MoS_2 were used as a transparent electrode by Hu et al. [226] AgNW-MoS_2 as a transparent electrode shows 93.1% transparency at 550 nm and gives lower values of sheet resistance (9.8 Ω/sq). MoS_2 in the AgNW-MoS_2 composite electrode helps to improve the environmental reliability and provides better resistance against oxidation and moisture as compared to the AgNW electrode alone. PBDTTT-C-T: PC70BM based organic solar cell gives PCE of 8.72% by using the anode of p-MoS_2 nanosheets/Ag for hole extraction and cathode of AgNWs-MoS_2 nanosheets/n-MoS_2 nanosheets for electron extraction. General cell configuration, in this case, is glass/AgNW-MoS_2/n-MoS_2/PBDTTT-C-T: PC70BM/p-MoS_2/Ag being sketched in Figure 4a. MoS_2 in combination with MoO_3 and MoS_2 with Au nanoparticles were also used as hole extraction layers in organic solar cells by Qin et al. [227] and Yang et al. [228] respectively. Chuang et al. [229] used nanosheets of MoS_2 along with Au nanoparticles as an electron extraction layer and obtained PCE of 4.91%.

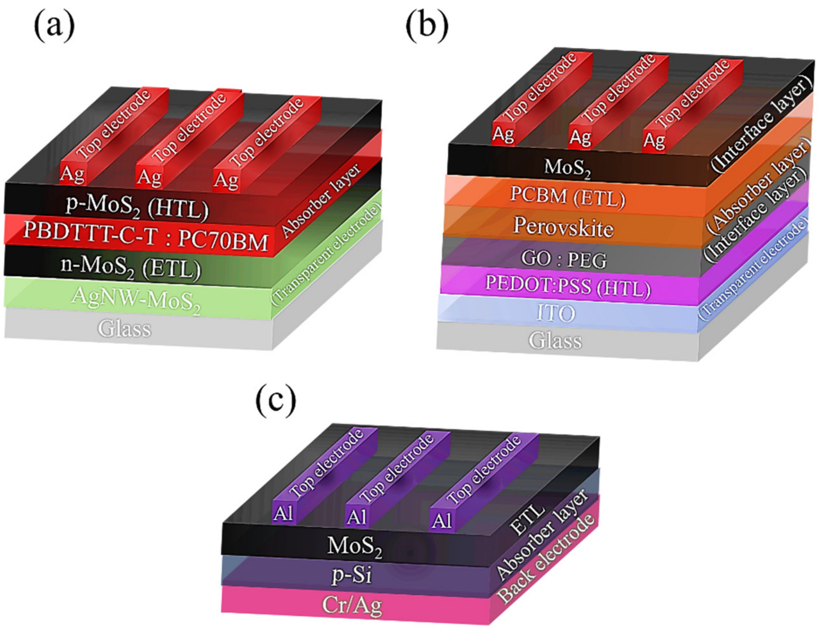

Figure 4. (**a**) An easy sketching of glass/AgNW-MoS_2/n-MoS_2/PBDTTT-C-T:PC70BM/p-MoS_2/Ag based organic solar cell [226]. (**b**) ITO/PEDOT:PSS/GO/perovskite/PCBM/MoS_2/Ag based perovskite solar cell [230]. (**c**) MoS_2/p-Si based heterojunction solar cells [231].

4.4. MoS_2 Efficient Role in Perovskite Solar Cells

The generic formula of perovskite solar cells is ABX_3. Most commonly in organometallic halide perovskites solar cells, A is $CH_3NH_3^+$ and B is Pb. Whereas X is an anion which is a halogen (Cl, Br, I) [232]. For separation and collection of generated charges, electron and hole extraction layers are inserted between the active layer and electrodes. Spiro-OMeTAD (2,2′,7,7′-tetrakis(*N*,*N*-di-*p*-methoxyphenyl-amine)9,9′-spirobifluoren) mostly used as hole transport material in perovskite solar cells because HOMO of Spiro-OMeTAD and valence band maxima of $CH_3NH_3PBI_3$ has energy levels at 5.03 eV and 5.04 eV respectively. Spiro-OMeTAD productively conduct holes from the active layer ($CH_3NH_3PBI_3$) to the anode, but it is not cost-effective. That is why a number of other materials were used in its place in perovskite solar cells such as poly(3-hexylthiophene) P3HT [232,233], graphene oxide (GO) [234], poly(3,4-ethylene dioxythiophene) polystyrene sulfonate (PEDOT:PSS) [235], reduced graphene oxide (rGO) [236,237], copper(I) iodide (CuI) [238] and MoS_2 [239], etc.

Kim et al. [240] deliberated the hole transfer characteristic of MoS_2. The work function of MoS_2 (4.95 eV) is in the same league as PEDOT: PSS (5.25 eV), consequently, MoS_2 can also be used as a hole transfer layer in perovskite solar cells. Kim et al. [240] reported a PCE of 9.53% for MoS_2-based devices. Capasso et al. [241] used MoS_2 as HEL in perovskite solar cell that gives PCE of 3.95% as compared to the PCE of 3.1% obtained using spiro-OMeTAD (3.1%). MoS_2 monolayer incorporated in perovskite solar cells to give protection and hole transportation. Furthermore, few layers of MoS_2 (3 nm thick) nanosheets can be used to protect the short circuit between the two electrodes and to conduct the holes from the active layer (perovskite) to spiro-OMeTAD. Power conversion efficiency (PCE) of perovskite solar cell increases to 16.47%, by mixing MoS_2 with PEDOT: PSS and used as a hole transfer layer, as compared to PCE of (14.69%) obtained by using PEDOT: PSS solely. Capasso et al. [242] revealed that in the configuration of glass/FTO/compact-TiO_2/mesoporous-TiO_2/$CH_3NH_3PBI_3$/MoS_2/Spiro-OMeTAD/Au solar cell, PCE of 13.3% can be obtained with higher stability.

Wang et al. [230] used MoS_2 and GO in perovskite solar cell and cell configuration was ITO/PEDOT: PSS/GO/perovskite/PCBM/MoS_2/Ag as shown in Figure 4b. Using $MAPbI_3$ as an active layer, PCE achieved was 19.14%, increased from 14.15% with VOC of 1.135 V, increased from 0.962 V. Dasgupta et al. [239] used p-type doped MoS_2 in perovskite solar cells containing $MAPbI_3$ and reported

6.01% PCE. Huang et al. [243] used MoS_2 as hole transport material in perovskites and achieved PCE of 15.4% and by using WS_2 as HTL, PCE of 20% achieved. The higher photon conversion efficiency of TMDCs is due to the well-aligned valence band of specific TMDC and perovskite material, lower value of series resistance, and higher shunt resistance. Kakavelakis et al. [244] incorporated MoS_2 as an interlayer between active layers (perovskite material) and hole transport layer (PTAA) and enhance the efficiency of perovskite solar cells by 6% as compared to the perovskite solar cells without MoS_2. Kohnehpoushi et al. [245] also used MoS_2 as a hole withdrawal layer in $MAPbI_3$ containing perovskite solar cells and reported PCE of 20.53%.

Ahmed et al. [246] used a composite of MoS_2 with TiO_2 as an electron extraction layer in perovskite solar cells. MoS_2/TiO_2 composite enhanced the absorption range of solar cells from 350 to 800 nm. Power conversion efficiency (PCE) obtained was increased from 3.74% to 4.43% as compared to pure TiO_2 based perovskite solar cells.

4.5. MoS_2 in Silicon-Based Heterojunction Solar Cells

2D materials exhibit distinctive optoelectronic features that are appropriate for manufacturing 2D-materials based solar cells. Among TMDCs, MoS_2 shows fascinating optoelectronic attributes and its band gap influenced by the number of layers [247–249]. Abundant research has been accompanied related to optoelectronic characteristics, conversion of solar energy, light emission, and heterostructures of TMDCs [250–252].

Shanmugam et al. [231] manufactured Schottky-barrier solar cells. Nanomembranes of MoS_2 were used as a photoactive layer and PCE of 0.7% was achieved for MoS_2 with 110 nm thickness using ITO/MoS_2/Au based solar cell. For 220 nm thick MoS_2 based solar cells, PCE of 1.8% was achieved. A similar group reported PCE of 1.3% using ITO/TiO_2/MoS_2/P3HT/Au based bulk heterojunction solar cells. Tsai et al. [231] utilized monolayer of n-MoS_2 with the p-silicon substrate to fabricate heterojunction based solar cells. Al/MoS_2/p-Si/Cr-Ag based heterojunction solar cell gave J_{SC} of 22.36 mA/cm^2, PCE of 5.23%, fill factor (FF) of 57.26% and VOC of 0.41 V in contrast to J_{SC} of 21.66 mA/cm^2,FF of 56.02% and VOC of 0.38 V for Al/p-Si based solar cells. Figure 4c is the simplified sketching of Al/MoS_2/p-Si/Cr-Ag based heterojunction solar cell [231]. Hao et al. [253] fabricated p–n junction based MoS_2/Si solar cells. MoS_2 transferred to the p-type silicon substrate by magnetron sputtering and gave VOC of 0.14 V, PCE of 1.3%, FF of 42.4%, and Jsc of 3.2 mA/cm^2. To overcome the transfer process of the as-synthesized MoS_2 layer on the substrate, Hasani et al. [254] synthesized MoS_2 directly on substrate in n-MoS_2/p-Si-based heterostructure device.

Jiao et al. [255] studied the effect of MoS_2 in graphene/silicon-based solar cells. MoS_2 performed the function of the interfacial layer in this scenario and gave PCE of 4.4%. Jiao et al. [255] also studied the effect of annealing temperature on the MoS_2 prototype which affects the PCE of the device. The same group reported PCE of 6.6% achieved by silicon substrate surface passivation. Hao et al. [256] deposited MoS_2 on p-type silicon substrate buffered with SiO_2. They studied photovoltaic features of Pd/MoS_2/(3−5 nm) SiO_2/Si/based heterojunction solar cell with SiO_2 buffer layer and without SiO_2 buffer layer. MoS_2/Si based heterojunction solar cell gave PCE of 1.4% and after incorporation of SiO_2 buffer, layer PCE increased by three-fold (4.5%). Buffer layer reduces the chances of recombination of electrons and holes. PCE of 15.8% was achieved by using MoS_2 in graphene/silicon solar cells [252]. Graphene/MoS_2/Si based heterojunction solar cell gave a better performance like Jsc of 26.6 mA/cm^2, FF of 62% and VOC of 0.50 V as compared to the device without MoS_2 with open-circuit voltage (VOC) of 0.45 V, fill factor (FF) of 54% and short-circuit current density (Jsc) of 25.6 mA/cm^2.

Tsuboi et al. [257] used MoS_2 between graphene and silicon substrate as an electron blocking and passivation layer in graphene/MoS_2/n-Si-based heterojunction solar cells. Higher PCE of 1.35% was achieved with MoS_2 as compared to PCE of 0.07% without the incorporation of MoS_2 in the device. PCE increased to 8.0% by using tri-layer graphene in the solar cell. Power conversion efficiency (PCE) increased by increasing the number of layers of graphene. MoS_2 with a thickness of 9 nm in tri-layer graphene/MoS_2/n-Si-based heterojunction solar cells gave PCE of 11.1%. Van der Waals based MoS_2/WSe_2 heterostructures being fabricated by Furchi et al. [258] on SiO_2/silicon substrate. Graphene/MoS_2 and WS_2/MoS_2 heterostructures have gained research interest as they carry a powerful role in electronic appliances [259–263]. Al_2O_3 used as passivation layer in MoS_2/silicon-based heterojunction solar cell [264]. Power conversion efficiency (PCE) of 5.6% can be obtained by passivating MoS_2 surface by Al_2O_3 as compared to PCE of 2.21% achieved by MoS_2/silicon-based device without Al_2O_3 passivation layer.

MoS_2/silicon heterojunction solar cell was fabricated by the direct buildup of MoS_2 on the substrate by the sol-gel method [265]. ITO/MoS_2/p-Si/Ag-based solar cell showed enhanced photovoltaic performance. By in situ growth of MoS_2, defects at the interface were reduced, higher VOC accredited to the emergence of heterojunction at Mos_2/silicon interface and due to reduction in defects at interface, recombination losses also decreased, consequently Jsc increased. Mueller and coworkers [258] fabricated WSe_2/MoS_2 based heterostructure and achieved a power conversion efficiency of 0.2%. In bulk heterojunction solar cells, the major restriction is limited absorption range (≈100–200 nm) of polymers as compared to silicon. To get better absorption and performance of solar cells, tandem solar cells evolved. Several single-junction based solar cells piled up vertically in tandem solar cell design [266]. This stacking reduces the thermalization effect because each part of the vertical stack absorbs a specific part of sunlight. Saraswat et al. [267] manufactured most effective TMDCs/silicon-based tandem solar cells.

5. Summary and Outlook

Here, in this review, we have summed up the subclasses of 2Ds with their respective crystalline structures, synthetic strategies, optoelectric properties, and applications of TMDCs particularly MoS_2 in solar cell devices. Functioning of MoS_2, specifically in DSSCs, Organic solar cells, perovskite solar cells, and in silicon heterojunction solar cells has been briefly analyzed in this review. 2D materials, especially TMDCs having fascinating properties, come up with great research interest to cater the innovative opportunities among research groups to investigate the concepts and phenomena in energy, electronics, and optoelectronics. Taking into consideration, authentic fabrication methods have developed for 2D materials including micromechanical cleavage strategy, which offers high-quality nanosheets, but this method is known with lab-scale production and cannot cope with industrial needs. Along with micromechanical cleavage, liquid-based exfoliation, electrochemical exfoliation, and CVD also give reliable results for different applications. Graphene-affiliated research has been reached in maturity after an in-depth investigation of many years. Now, layered TMDCs provoking new thrill in research because of their captivating properties such as cost-effective, tunable work function, catalytic effect, high absorption coefficient, strong light-matter interaction, and thickness-dependent bandgap. Due to the atomically thin layered structure, enhanced optical and electric properties, TMDCs have a wide range of applications in photovoltaic devices. MoS_2, in DSSCs, can be used as a counter electrode replacing conventional expensive and less stable platinum counter electrode and gives enhanced power conversion efficiency of 7.50% as compared to the platinum electrode. To fulfill increasing energy demands, third-generation solar cells, organic and perovskite, play a vital role. Due to the tunability of work function, MoS_2 can be used as both an electron extractor and a hole extractor layer in organic and perovskite solar cells. MoS_2 can be used as a buffer layer, interfacial layer, electron transport layer, and as a hole transport layer in organic solar cells. Power conversion efficiency (PCE) of 8.43% achieved by using MoS_2 in organic solar cells. MoS_2 in perovskite solar cells exhibited a power conversion efficiency of 9.53%, higher than the device containing PEDOT: PSS as the hole transport layer. In another scenario of perovskites, TiO_2/$CH_3NH_3PbI_3$/MoS_2/Spiro-OMeTAD/Au, PCE of 13.3% was achieved. Perovskite solar cells incorporating MoS_2 gave PCE of 20.4%. In the present literature survey, heterojunction solar cells are also analyzed. 2D (two-dimensional) /2D van der Waals heterostructures enhance watt per gram usage of photo-active material. Graphene/MoS_2, WS_2/MoS_2, and MoS_2/Si based heterojunction solar cells with varying values of power conversion efficiencies have also been summarized there. A large number of research groups are working on the emerging field of TMDCs, but still, in many ways, this field is in premature stage with various transition metal dichalcogenides which are not investigated and fabricated yet and which could be the source of the novel as well as enchanting discoveries. More research should pay attention to incorporating TMDCs in various types of solar cells to enhance the PCE.

Funding: This research received no external funding.

Conflicts of Interest: The authors declare no conflict of interest.

References

1. Geim, A.K.; Novoselov, K.S.; Jiang, D.; Schedin, F.; Booth, T.J.; Khotkevich, V.V.; Morozov, S.V. Two-dimensional atomic crystals. *Proc. Natl. Acad. Sci. USA* **2005**, *102*, 10451–10453.
2. Novoselov, K.S.; Mishchenko, A.; Carvalho, A.; Castro Neto, A.H. 2D materials and van der Waals heterostructures. *Science* **2016**, *353*, 6298. [CrossRef] [PubMed]
3. Butler, S.Z.; Hollen, S.M.; Cao, L.; Cui, Y.; Gupta, J.A.; Gutiérrez, H.R.; Heinz, T.F.; Hong, S.S.; Huang, J.; Ismach, A.F.; et al. Progress, challenges, and opportunities in two-dimensional materials beyond graphene. *ACS Nano* **2013**, *7*, 2898–2926. [CrossRef] [PubMed]
4. Lauhon, L.J.; Marks, T.J.; Hersam, M.C.; Sangwan, V.K.; Jariwala, D. Emerging Device Applications for Semiconducting Two-Dimensional Transition Metal Dichalcogenides. *ACS Nano* **2014**, *8*, 1102–1120.
5. Duan, X.; Wang, C.; Pan, A.; Yu, R.; Duan, X. Two-dimensional transition metal dichalcogenides as atomically thin semiconductors: Opportunities and challenges. *Chem. Soc. Rev.* **2015**, *44*, 8859–8876. [CrossRef]
6. Zhang, H. Introduction: 2D Materials Chemistry. *Chem. Rev.* **2018**, *118*, 6089–6090. [CrossRef]
7. Zhang, H.; Cheng, H.M.; Ye, P. 2D nanomaterials: Beyond graphene and transition metal dichalcogenides. *Chem. Soc. Rev.* **2018**, *47*, 6009–6012. [CrossRef]
8. Li, X.; Wu, X. Low-dimensional boron nitride nanomaterials. *J. Univ. Sci. Technol. China* **2014**, *44*, 389–402.
9. Wang, Z.F.; Liu, F.; Wu, D.; Jin, C.; Li, Y.; Storr, K.; Srivastava, A.; Balicas, L.; Ajayan, P.M.; Ci, L.; et al. Atomic layers of hybridized boron nitride and graphene domains. *Nat. Mater.* **2010**, *9*, 430–435.
10. Vogt, P.; De Padova, P.; Quaresima, C.; Avila, J.; Frantzeskakis, E.; Asensio, M.C.; Resta, A.; Ealet, B.; Le Lay, G. Silicene: Compelling experimental evidence for graphenelike two-dimensional silicon. *Phys. Rev. Lett.* **2012**, *108*, 1–5. [CrossRef]
11. Tan, C.; Cao, X.; Wu, X.J.; He, Q.; Yang, J.; Zhang, X.; Chen, J.; Zhao, W.; Han, S.; Nam, G.H.; et al. Recent Advances in Ultrathin Two-Dimensional Nanomaterials. *Chem. Rev.* **2017**, *117*, 6225–6331. [CrossRef]
12. Choi, W.; Choudhary, N.; Han, G.H.; Park, J.; Akinwande, D.; Lee, Y.H. Recent development of two-dimensional transition metal dichalcogenides and their applications. *Mater. Today.* **2017**, *20*, 116–130. [CrossRef]
13. Colombo, L.; Kim, K.; Gellert, P.R.; Novoselov, K.S.; Fal'ko, V.I.; Schwab, M.G. A roadmap for graphene. *Nature* **2012**, *490*, 192–200.
14. Fivaz, R.; Mooser, E. Mobility of charge carriers in semiconducting layer structures. *Phys. Rev.* **1967**, *163*, 743–755. [CrossRef]
15. Tributsch, H.; Bennett, J.C. Electrochemistry and photochemistry of MoS_2 layer crystals. I. *J. Electroanal. Chem.* **1977**, *81*, 97–111. [CrossRef]
16. Wang, H.; Liu, F.; Fu, W.; Fang, Z.; Zhou, W.; Liu, Z. Two-dimensional heterostructures: Fabrication, characterization, and application. *Nanoscale* **2014**, *6*, 12250–12272. [CrossRef] [PubMed]
17. Zhu, Y.; Murali, S.; Cai, W.; Li, X.; Suk, J.W.; Potts, J.R.; Ruoff, R.S. Graphene and graphene oxide: Synthesis, properties, and applications. *Adv. Mater.* **2010**, *22*, 3906–3924. [CrossRef] [PubMed]
18. Chrisey, D.B.; Mattoussi, H.; Gilmore, C.M.; Horwitz, J.S.; Kim, H.; Kafafi, Z.H.; Piqué, A.; Murata, H. Electrical, optical, and structural properties of indium–tin–oxide thin films for organic light-emitting devices. *J. Appl. Phys.* **2002**, *86*, 6451–6461.
19. Gusakova, J.; Wang, X.; Shiau, L.L.; Krivosheeva, A.; Shaposhnikov, V.; Borisenko, V.; Gusakov, V.; Tay, B.K. Electronic Properties of Bulk and Monolayer TMDs: Theoretical Study Within DFT Framework (GVJ-2e Method). *Phys. Status Solidi Appl. Mater. Sci.* **2017**, *214*, 1–7. [CrossRef]
20. Toth, P.S. From two-dimensional materials to their heterostructures: An electrochemist's perspective. *Appl. Mater. Today* **2017**, *8*, 68–103.

21. Pumera, M.; Sofer, Z.; Ambrosi, A. Layered transition metal dichalcogenides for electrochemical energy generation and storage. *J. Mater. Chem. A* **2014**, *2*, 8981–8987. [CrossRef]
22. Xiao, J.; Long, M.; Li, X.; Zhang, Q.; Xu, H.; Chan, K.S. Effects of van der Waals interaction and electric field on the electronic structure of bilayer MoS_2. *J. Phys. Condens. Matter* **2014**, *26*, 405302. [CrossRef] [PubMed]
23. Wang, Q.H.; Kalantar-Zadeh, K.; Kis, A.; Coleman, J.N.; Strano, M.S. Electronics and optoelectronics of two-dimensional transition metal dichalcogenides. *Nat. Nanotechnol.* **2012**, *7*, 699–712.
24. Podberezskaya, N.V.; Magarill, S.A.; Pervukhina, N.V.; Borisov, S.V. Crystal chemistry of dichalcogenides MX. *J. Struct. Chem.* **2001**, *42*, 654–681. [CrossRef]
25. Li, X.; Zhu, H. Two-dimensional MoS_2: Properties, preparation, and applications. *J. Mater.* **2015**, *1*, 33–44. [CrossRef]
26. Mak, K.F.; Lee, C.; Hone, J.; Shan, J.; Heinz, T.F. Atomically thin MoS_2: A new direct-gap semiconductor. *Phys. Rev. Lett.* **2010**, *105*, 136805. [CrossRef]
27. Zhang, H. Ultrathin Two-Dimensional Nanomaterials. *ACS Nano* **2015**, *9*, 9451–9469. [CrossRef]
28. Cheng, R.; Jiang, S.; Chen, Y.; Liu, Y.; Weiss, N.; Cheng, H.C.; Wu, H.; Huang, Y.; Duan, X. Few-layer molybdenum disulfide transistors and circuits for high-speed flexible electronics. *Nat. Commun.* **2014**, *5*, 1–9. [CrossRef]
29. Akinwande, D.; Petrone, N.; Hone, J. Two-dimensional flexible nanoelectronics. *Nat. Commun.* **2014**, *5*, 1–12. [CrossRef]
30. Samadi, M.; Sarikhani, N.; Zirak, M.; Zhang, H.; Zhang, H.L.; Moshfegh, A.Z. Group 6 transition metal dichalcogenide nanomaterials: Synthesis, applications and future perspectives. *Nanoscale Horiz.* **2018**, *3*, 90–204. [CrossRef]
31. Fleischauer, P.D.; Lince, J.R.; Bertrand, P.A.; Bauer, R. Electronic Structure and Lubrication Properties of MoS_2: A Qualitative Molecular Orbital Approach. *Langmuir* **1989**, *5*, 1009–1015. [CrossRef]
32. Kumara, A.; Ahluwalia, P.K. Electronic structure of transition metal dichalcogenides monolayers 1H-MX2 (M = Mo, W; X = S, Se, Te) from ab-initio theory: New direct band gap semiconductors. *Eur. Phys. J. B* **2012**, *85*, 18–22. [CrossRef]
33. Thanh, T.D.; Chuong, N.D.; Van Hien, H.; Kshetri, T.; Tuan, L.H.; Kim, N.H.; Lee, J.H. Recent advances in two-dimensional transition metal dichalcogenides-graphene heterostructured materials for electrochemical applications. *Prog. Mater. Sci.* **2018**, *96*, 51–85. [CrossRef]
34. Ni, S.Z.; Chen, W. Two-dimensional transition metal dichalcogenides: Interface and defect engineering. *Chem Soc Rev Rev.* **2018**, *47*, 3100–3128.
35. Py, M.A.; Haering, R.R. Structural destabilization induced by lithium intercalation in MoS_2 and related compounds. *Can. J. Phys.* **1983**, *61*, 76–84. [CrossRef]
36. Lin, Y.-C.; Dumcenco, D.O.; Huang, Y.-S.; Suenaga, K. Atomic mechanism of the semiconducting-to-metallic phase transition in single-layered MoS_2. *Nat. Nanotechnol.* **2014**, *9*, 391–396.
37. Voiry, D.; Salehi, M.; Silva, R.; Fujita, T.; Chen, M.; Asefa, T.; Shenoy, V.B.; Eda, G.; Chhowalla, M. Conducting MoS_2 nanosheets as catalysts for hydrogen evolution reaction. *Nano Lett.* **2013**, *13*, 6222–6227. [CrossRef]
38. Al, R.S.; Tatsumi, Y.; Huang, S.; Limg, X.; Dresselhaus, M.S. Raman spectroscopy of transition metal dichalcogenides. *J. Phys. Condens. Matter* **2016**, *28*, 353002.
39. Zhang, S.; Zhang, N.; Zhao, Y.; Cheng, T.; Li, X.; Feng, R.; Xu, H.; Liu, Z.; Zhang, J.; Tong, L. Spotting the differences in two-dimensional materials-the Raman scattering perspective. *Chem. Soc. Rev.* **2018**, *47*, 3217–3240. [CrossRef]
40. Jung, J.; Bark, H.; Byun, D.; Lee, C.; Cho, D.H. Mechanical characterization of phase-changed single-layer MoS 2 sheets. *2D Mater.* **2019**, *6*, 025024. [CrossRef]
41. Berkdemir, A.; Gutiérrez, H.R.; Botello-Méndez, A.R.; Perea-López, N.; Elías, A.L.; Chia, C.I.; Wang, B.; Crespi, V.H.; López-Urías, F.; Charlier, J.C.; et al. Identification of individual and few layers of WS_2 using Raman Spectroscopy. *Sci. Rep.* **2013**, *3*, 1–8. [CrossRef]
42. Li, H.; Zhang, Q.; Yap, C.C.R.; Tay, B.K.; Edwin, T.H.T.; Olivier, A.; Baillargeat, D. From bulk to monolayer MoS_2: Evolution of Raman scattering. *Adv. Funct. Mater.* **2012**, *22*, 1385–1390. [CrossRef]
43. Han, S.A.; Bhatia, R.; Kim, S.-W. Synthesis, properties and potential applications of two-dimensional transition metal dichalcogenides. *Nano Converg.* **2015**, *2*, 17. [CrossRef]
44. Li, L.-J.; Eda, G.; Zhang, H.; Loh, K.P.; Shin, H.S.; Chhowalla, M. The chemistry of two-dimensional layered transition metal dichalcogenide nanosheets. *Nat. Chem.* **2013**, *5*, 263–275.

45. Park, S.; Ruoff, R.S. Synthesis and characterization of chemically modified graphenes. *Curr. Opin. Colloid Interface Sci.* **2015**, *20*, 322–328. [CrossRef]
46. Nicolosi, V.; Chhowalla, M.; Kanatzidis, M.G.; Strano, M.S.; Coleman, J.N. Liquid exfoliation of layered materials. *Science.* **2013**, *340*, 72–75. [CrossRef]
47. Cai, Z.; Liu, B.; Zou, X.; Cheng, H. Chemical Vapor Deposition Growth and Applications of Two- Dimensional Materials and Their Heterostructures. *Chem. Rev.* **2018**, *118*, 6091–6133. [CrossRef]
48. Hummers, W.S.; Offeman, R.E. Preparation of Graphitic Oxide. *J. Am. Chem. Soc.* **1958**, *80*, 1339. [CrossRef]
49. Li, H.; Wu, J.; Yin, Z.; Zhang, H. Preparation and applications of mechanically exfoliated single-layer and multilayer MoS_2 and WSe2 nanosheets. *Acc. Chem. Res.* **2014**, *47*, 1067–1075. [CrossRef]
50. Min Yi, Z.S. A review on mechanical exfoliation for the scalable production of graphene. *R. Soc. Chem.* **2015**, 11700–11715.
51. Narayan, R.; Kim, S.O. Surfactant mediated liquid phase exfoliation of graphene. *Nano Converg.* **2015**, *2*, 20. [CrossRef] [PubMed]
52. Dines, M.B. Lithium intercalation via n-Butyllithium of the layered transition metal dichalcogenides. *Mater. Res. Bull.* **1975**, *10*, 287–291. [CrossRef]
53. Parvez, K.; Wu, Z.S.; Li, R.; Liu, X.; Graf, R.; Feng, X.; Müllen, K. Exfoliation of Graphite into Graphene in Aqueous Solutions of Inorganic Salts. *J. Am. Chem. Soc.* **2014**, *136*, 6083–6091. [CrossRef] [PubMed]
54. Zheng, J.; Zhang, H.; Dong, S.; Liu, Y.; Nai, C.T.; Shin, H.S.; Jeong, H.Y. High yield exfoliation of two-dimensional chalcogenides using sodium naphthalenide. *Nat. Commun.* **2014**, *5*, 1–7. [CrossRef]
55. Zeng, Z.; Sun, T.; Zhu, J.; Huang, X.; Yin, Z.; Lu, G.; Fan, Z.; Yan, Q.; Hng, H.H.; Zhang, H. An Effective Method for the Fabrication of Few-Layer-Thick Inorganic Nanosheets. *Angew. Chem. Int. Ed.* **2012**, *51*, 9052–9056. [CrossRef] [PubMed]
56. Khan, U.; May, P.; Neill, A.O.; Bell, A.P.; Boussac, E.; Martin, A.; Coleman, J.N. Polymer reinforcement using liquid-exfoliated boron nitride nanosheets. *Nanoscale* **2013**, *5*, 581–587. [CrossRef] [PubMed]
57. Hernandez, Y.; Nicolosi, V.; Lotya, M.; Blighe, F.M.; Sun, Z.; De, S.; McGovern, I.T.; Holland, B.; Byrne, M.; Gun'ko, Y.K.; et al. High-yield production of graphene by liquid-phase exfoliation of graphite. *Nat. Nanotechnol.* **2008**, *3*, 563–568.
58. Niu, L.; Coleman, J.N.; Zhang, H.; Shin, H.; Chhowalla, M.; Zheng, Z. Production of Two-Dimensional Nanomaterials via Liquid-Based Direct Exfoliation. *Small* **2016**, *12*, 272–293. [CrossRef]
59. Halim, U.; Zheng, C.R.; Chen, Y.; Lin, Z.; Jiang, S.; Cheng, R.; Huang, Y.; Duan, X. A rational design of cosolvent exfoliation of layered materials by directly probing liquid-solid interaction. *Nat. Commun.* **2013**, *4*, 1–7. [CrossRef]
60. Stankovich, S.; Dikin, D.A.; Piner, R.D.; Kohlhaas, K.A.; Kleinhammes, A.; Jia, Y.; Wu, Y.; Nguyen, S.B.T.; Ruoff, R.S. Synthesis of graphene-based nanosheets via chemical reduction of exfoliated graphite oxide. *Carbon N. Y.* **2007**, *45*, 1558–1565. [CrossRef]
61. Lee, Y.; Zhang, X.; Zhang, W.; Chang, M.; Lin, C.; Chang, K.; Yu, Y.; Wang, J.T.; Chang, C.; Li, L.; et al. Synthesis of Large-Area MoS_2 Atomic Layers with Chemical Vapor Deposition. *Adv. Mater.* **2012**, *24*, 2320–2325. [CrossRef] [PubMed]
62. Reina, A.; Jia, X.; Ho, J.; Nezich, D.; Son, H.; Bulovic, V.; Dresselhaus, M.S.; Kong, J. Large Area, Few-Layer Graphene Films on Arbitrary Substrates by Chemical Vapor Deposition. *Nano Lett.* **2009**, *9*, 30–35. [CrossRef] [PubMed]
63. Yu, J.; Li, J.; Zhang, W.; Chang, H. Synthesis of high quality two-dimensional materials via chemical vapor deposition. *Chem. Sci.* **2015**, *6*, 6705–6716. [CrossRef] [PubMed]
64. Ji, Q.; Zheng, Y.; Zhang, Y.; Liu, Z. Chemical vapour deposition of group-VIB metal dichalcogenide monolayers: Engineered substrates from amorphous to single crystalline. *Chem. Soc. Rev.* **2015**, *44*, 2587–2602. [CrossRef]
65. Li, X.; Cai, W.; An, J.; Kim, S.; Nah, J.; Yang, D.; Piner, R.; Velamakanni, A.; Jung, I.; Tutuc, E.; et al. Large-area synthesis of high-quality and uniform graphene films on copper foils. *Science* **2009**, *324*, 1312–1314. [CrossRef]
66. Cheng, L.; Yuan, C.; Shen, S.; Yi, X.; Gong, H.; Yang, K.; Liu, Z. Bottom-up Synthesis of Metal-Ion-Doped WS_2 Nanoflakes for Cancer Theranostics. *ACS Nano* **2015**, *9*, 11090–11101. [CrossRef]
67. Lhuillier, E.; Pedetti, S.; Ithurria, S.; Nadal, B.; Heuclin, H.; Dubertret, B. Two-Dimensional colloidal metal chalcogenides semiconductors: Synthesis, spectroscopy, and applications. *Acc. Chem. Res.* **2015**, *48*, 22–30. [CrossRef]

68. Gebreegziabher, G.G.; Asemahegne, A.S.; Ayele, D.W.; Dhakshnamoorthy, M.; Kumar, A. One-step synthesis and characterization of reduced graphene oxide using chemical exfoliation method. *Mater. Today Chem.* **2019**, *12*, 233–239. [CrossRef]
69. Son, J.S.; Yu, J.H.; Kwon, S.G.; Lee, J.; Joo, J.; Hyeon, T. Colloidal synthesis of ultrathin two-dimensional semiconductor nanocrystals. *Adv. Mater.* **2011**, *23*, 3214–3219. [CrossRef]
70. Yang, Y.; Hou, H.; Zou, G.; Shi, W.; Shuai, H.; Li, J.; Ji, X. Electrochemical exfoliation of graphene-like two-dimensional nanomaterials. *Nanoscale* **2019**, *11*, 16–33. [CrossRef]
71. Ambrosi, A.; Pumera, M. Electrochemical Exfoliation of MoS_2 Crystal for Hydrogen Electrogeneration. *Chem. Eur. J.* **2018**, *24*, 18551–18555. [CrossRef] [PubMed]
72. Schedy, A.; Quarthal, D.; Oetken, M. Graphene—Exciting Insights into the Synthesis and Chemistry of the Miracle Material of the 21st Century and Its Implementation in Chemistry Lessons for the First Time. *World J. Chem. Educ.* **2018**, *6*, 43–53. [CrossRef]
73. Chakrabarti, M.H.; Low, C.T.J.; Brandon, N.P.; Yufit, V.; Hashim, M.A.; Irfan, M.F.; Akhtar, J.; Ruiz-trejo, E.; Hussain, M.A. Electrochimica Acta Progress in the electrochemical modification of graphene-based materials and their applications. *Electrochim. Acta* **2013**, *107*, 425–440. [CrossRef]
74. Schulman, D.S.; Sebastian, A.; Buzzell, D.; Huang, Y.T.; Arnold, A.J.; Das, S. Facile Electrochemical Synthesis of 2D Monolayers for High-Performance Thin-Film Transistors. *ACS Appl. Mater. Interfaces* **2017**, *9*, 44617–44624. [CrossRef]
75. Buzaglo, M.; Bar, I.P.; Varenik, M.; Shunak, L.; Pevzner, S.; Regev, O. Graphite-to-Graphene: Total Conversion. *Adv. Mater.* **2017**, *29*, 1–5. [CrossRef]
76. Naguib, M.; Halim, J.; Lu, J.; Cook, K.M.; Hultman, L.; Gogotsi, Y.; Barsoum, M.W. New two-dimensional niobium and vanadium carbides as promising materials for li-ion batteries. *J. Am. Chem. Soc.* **2013**, *135*, 15966–15969. [CrossRef]
77. Naguib, M.; Kurtoglu, M.; Presser, V.; Lu, J.; Niu, J.; Heon, M.; Hultman, L.; Gogotsi, Y.; Barsoum, M.W. Two-dimensional nanocrystals produced by exfoliation of Ti3AlC. *Adv. Mater.* **2011**, *23*, 4248–4253. [CrossRef]
78. Naguib, M.; Mashtalir, O.; Carle, J.; Presser, V.; Lu, J.; Hultman, L.; Gogotsi, Y.; Barsoum, M.W. Two-dimensional transition metal carbides. *ACS Nano* **2012**, *6*, 1322–1331. [CrossRef]
79. Thakare, S.R.; Fendarkar, D.A.; Bidkar, C.; Yadav, J.; Gedam, S.D. Chemical Functionalization of Graphene and Graphene Oxide—A Review. *Issn* **2017**, *5*, 1–23.
80. Singh, N.; Kalotra, P.; Srivastava, S.; Sharma, S.S. Comparative Study for the Synthesis of Graphene Oxide from Different Chemical Routes. *Adv. Sci. Eng. Med.* **2019**, *11*, 92–94. [CrossRef]
81. Roberts, E.P.L.; Sharif, F.; Holmes, S.; Perez-page, M. Synthesis of Graphene by Electrochemical Exfoliation of Graphite in Aqueous Solution. *ECS Meet. Abstr.* **2018**, *MA2018-02*, 546.
82. Lin, L. Graphene Synthesis via Electrochemical Exfoliation of Graphite Nanoplatelets in Aqueous Sulfuric Acid. In Proceedings of the CARBON 2016, Graphene Characterisation Protocol, State College, PA, USA, 10–15 July 2016.
83. Gu, X.; Zhao, Y.; Sun, K.; Vieira, C.L.Z.; Jia, Z.; Cui, C.; Wang, Z.; Walsh, A.; Huang, S. Method of ultrasound-assisted liquid-phase exfoliation to prepare graphene. *Ultrason. Sonochem.* **2019**, *58*, 104630. [CrossRef] [PubMed]
84. Spanu, L.; Sorella, S.; Galli, G. Nature and Strength of Interlayer Binding in Graphite. *Phys. Rev. Lett.* **2009**, *103*, 1–4. [CrossRef] [PubMed]
85. Alba, A. Enfermedad De Vogt-Koyanagi-Harada. *Seminarios de la Fundación Española de Reumatología* **1999**, *1906*, 666–670.
86. Li, H.; Lu, G.; Wang, Y.; Yin, Z.; Cong, C.; He, Q.; Wang, L. Mechanical Exfoliation and Characterization of Single- and Few-Layer Nanosheets of WSe 2, TaS 2, and TaSe 2. *Small* **2013**, 1974–1981. [CrossRef]
87. Geim, A.K. Nobel Lecture: Random walk to graphene. *Rev. Mod. Phys.* **2011**, *83*, 851–862. [CrossRef]
88. Dresselhaus, M.S.; Araujo, P.T. Perspectives on the 2010 Nobel Prize in physics for graphene. *ACS Nano* **2010**, *4*, 6297–6302. [CrossRef]
89. Alem, N.; Erni, R.; Kisielowski, C.; Rossell, M.D.; Gannett, W.; Zettl, A. Atomically thin hexagonal boron nitride probed by ultrahigh-resolution transmission electron microscopy. *Phys. Rev. B* **2009**, *80*, 155425. [CrossRef]
90. Wang, F.; Wang, Z.; Wang, Q.; Wang, F.; Yin, L.; Xu, K.; Huang, Y.; He, J. Synthesis, properties and applications of 2D non-graphene materials. *Nanotechnology* **2015**, *26*, 292001. [CrossRef]

91. Huang, Y.; Sutter, E.; Shi, N.N.; Zheng, J.; Yang, T.; Englund, D.; Gao, H.J.; Sutter, P. Reliable Exfoliation of Large-Area High-Quality Flakes of Graphene and Other Two-Dimensional Materials. *ACS Nano* **2015**, *9*, 10612–10620. [CrossRef]
92. Brodie, B.C., XIII. On the atomic weight of graphite. *R. Soc.* **1859**, *149*, 249–259. [CrossRef]
93. Staudenmaier, L. Verfahren zur Darstellung der Graphitsäure. *Berichte der Dtsch. Chem. Gesellschaft* **1898**, *31*, 1481–1487. [CrossRef]
94. Gao, W. *Graphite Oxide: Structure, Reduction and Applications*; RICE University: Houston, TX, USA, 2012.
95. Chua, C.K.; Pumera, M. Chemical reduction of graphene oxide: A synthetic chemistry viewpoint. *Chem. Soc. Rev.* **2014**, *43*, 291–312. [CrossRef] [PubMed]
96. Hofmann, U.; König, E. Untersuchungen über Graphitoxyd. *Zeitschrift für Anorg. und Allg. Chem.* **1937**, *234*, 311–336. [CrossRef]
97. Peng, L.; Xu, Z.; Liu, Z.; Wei, Y.; Sun, H.; Li, Z.; Zhao, X.; Gao, C. An iron-based green approach to 1-h production of single-layer graphene oxide. *Nat. Commun.* **2015**, *6*, 1–9. [CrossRef]
98. Blanco, P.; Granda, M.; Blanco, C.; Botas, C.; Patricia, A.; Romasanta, L.J.; Verdejo, R.; Mene, R.; Lo, M.A. Graphene materials with different structures prepared from the same graphite by the Hummers and Brodie methods. *Carbon N. Y.* **2013**, *65*, 156–164.
99. Chen, J.; Yao, B.; Li, C.; Shi, G. An improved Hummers method for eco-friendly synthesis of graphene oxide. *Carbon N. Y.* **2013**, *64*, 225–229. [CrossRef]
100. Marcano, D.C.; Kosynkin, D.V.; Berlin, J.M.; Sinitskii, A.; Sun, Z.; Slesarev, A.; Alemany, L.B.; Lu, W.; Tour, J.M. Improved Synthesis of Graphene Oxide. *ACS Nano* **2010**, *4*, 4806–4814. [CrossRef]
101. Alam, S.N.; Sharma, N.; Kumar, L. Synthesis of Graphene Oxide (GO) by Modified Hummers Method and Its Thermal Reduction to Obtain Reduced Graphene Oxide (rGO)*. *Graphene* **2017**, *6*, 1–18. [CrossRef]
102. Zaaba, N.I.; Foo, K.L.; Hashim, U.; Tan, S.J.; Liu, W.W.; Voon, C.H. Synthesis of Graphene Oxide using Modified Hummers Method: Solvent Influence. *Procedia Eng.* **2017**, *184*, 469–477. [CrossRef]
103. Sohail, M.; Saleem, M.; Ullah, S.; Saeed, N.; Afridi, A.; Khan, M.; Arif, M. Modified and improved Hummer's synthesis of graphene oxide for capacitors applications. *Mod. Electron. Mater.* **2017**, *3*, 110–116. [CrossRef]
104. Romero, A.; Lavin-Lopez, M.P.; Sanchez-Silva, L.; Valverde, J.L.; Paton-Carrero, A. Comparative study of different scalable routes to synthesize graphene oxide and reduced graphene oxide. *Mater. Chem. Phys.* **2018**, *203*, 284–292. [CrossRef]
105. Yu, H.; Zhang, B.; Bulin, C.; Li, R.; Xing, R. High-efficient Synthesis of Graphene Oxide Based on Improved Hummers Method. *Sci. Rep.* **2016**, *6*, 1–7. [CrossRef] [PubMed]
106. Guerrero-Contreras, J.; Caballero-Briones, F. Graphene oxide powders with different oxidation degree, prepared by synthesis variations of the Hummers method. *Mater. Chem. Phys.* **2015**, *153*, 209–220. [CrossRef]
107. Gao, W. The chemistry of graphene oxide. In *Graphene Oxide*; Springer: Berlin/Heidelberg, Germany, 2015; pp. 61–95.
108. Fan, X.; Peng, W.; Li, Y.; Li, X.; Wang, S.; Zhang, G.; Zhang, F. Deoxygenation of Exfoliated Graphite Oxide under Alkaline Conditions: A Green Route to Graphene Preparation. *Adv. Mater.* **2008**, *20*, 4490–4493. [CrossRef]
109. Williams, G.; Seger, B.; Kamat, P.V. TiO2-Graphene Nanocomposites. UV-Assisted Photocatalytic Reduction of Graphene Oxide. *ACS Nano* **2008**, *2*, 1487–1491. [CrossRef] [PubMed]
110. Wang, Z.; Zhou, X.; Zhang, J.; Boey, F.; Zhang, H. Direct electrochemical reduction of single-layer graphene oxide and subsequent functionalization with glucose oxidase. *J. Phys. Chem. C* **2009**, *113*, 14071–14075. [CrossRef]
111. Smith, A.T.; LaChance, A.M.; Zeng, S.; Liu, B.; Sun, L. Synthesis, properties, and applications of graphene oxide/reduced graphene oxide and their nanocomposites. *Nano Mater. Sci.* **2019**, *1*, 31–47. [CrossRef]
112. Emiru, T.F.; Ayele, D.W. Controlled synthesis, characterization and reduction of graphene oxide: A convenient method for large scale production. *Egypt. J. Basic Appl. Sci.* **2017**, *4*, 74–79. [CrossRef]
113. Ghorbani, M.; Abdizadeh, H.; Golobostanfard, M.R. Reduction of Graphene Oxide via Modified Hydrothermal Method. *Procedia Mater. Sci.* **2015**, *11*, 326–330. [CrossRef]
114. Jung, I.; Dikin, D.A.; Piner, R.D.; Ruoff, R.S. Tunable Electrical Conductivity of Individual Graphene Oxide Sheets Reduced at Low Temperatures. *Nano Lett.* **2008**, *8*, 1–5. [CrossRef]
115. Kim, F.; Cote, L.J.; Huang, J. Graphene oxide: Surface activity and two-dimensional assembly. *Adv. Mater.* **2010**, *22*, 1954–1958. [CrossRef] [PubMed]

116. Bi, H.; Xie, X.; Yin, K.; Zhou, Y.; Wan, S.; He, L.; Xu, F.; Banhart, F.; Sun, L.; Ruoff, R.S. Spongy graphene as a highly efficient and recyclable sorbent for oils and organic solvents. *Adv. Funct. Mater.* **2012**, *22*, 4421–4425. [CrossRef]
117. Liu, N.; Luo, F.; Wu, H.; Liu, Y.; Zhang, C.; Chen, J. One-Step Ionic-Liquid-Assisted Electrochemical Synthesis of Ionic-Liquid-Functionalized Graphene Sheets Directly from Graphite**. *Adv. Funct. Mater.* **2008**, *18*, 1518–1525. [CrossRef]
118. Lu, J.; Yang, J.; Wang, J.; Lim, A.; Wang, S.; Loh, K.P. One-Pot Synthesis of Fluorescent Carbon Nanoribbons, Nanoparticles, and Graphene by the Exfoliation of Graphite in Ionic Liquids. *ACS Nano* **2009**, *3*, 2367–2375. [CrossRef]
119. You, X.; Chang, J.H.; Ju, B.K.; Pak, J.J. An electrochemical route to graphene oxide. *J. Nanosci. Nanotechnol.* **2011**, *11*, 5965–5968. [CrossRef]
120. Su, C.Y.; Lu, A.Y.; Xu, Y.; Chen, F.R.; Khlobystov, A.N.; Li, L.J. High-quality thin graphene films from fast electrochemical exfoliation. *ACS Nano* **2011**, *5*, 2332–2339. [CrossRef]
121. Tripathi, P.; Patel, C.R.P.; Shaz, M.A.; Srivastava, O.N. Synthesis of High-Quality Graphene through Electrochemical Exfoliation of Graphite in Alkaline Electrolyte. *arXiv* **2013**, arXiv:1310.7371.
122. Parvez, K.; Li, R.; Puniredd, S.R.; Hernandez, Y.; Hinkel, F.; Wang, S.; Feng, X.; Mu, K.; Engineering, C.; Road, D. Electrochemically Exfoliated Graphene as Solution-Processable, Highly Conductive Electrodes for Organic Electronics. *ACS Nano* **2013**, *7*, 3598–3606. [CrossRef]
123. Zhou, M.; Tang, J.; Cheng, Q.; Xu, G.; Cui, P.; Qin, L.C. Few-layer graphene obtained by electrochemical exfoliation of graphite cathode. *Chem. Phys. Lett.* **2013**, *572*, 61–65. [CrossRef]
124. Kakaei, K.; Hasanpour, K. Synthesis of graphene oxide nanosheets by electrochemical exfoliation of graphite in cetyltrimethylammonium bromide and its application for oxygen reduction. *J. Mater. Chem. A* **2014**, *2*, 15428–15436. [CrossRef]
125. Rao, K.S.; Senthilnathan, J.; Liu, Y.F.; Yoshimura, M. Role of peroxide ions in formation of graphene nanosheets by electrochemical exfoliation of graphite. *Sci. Rep.* **2014**, *4*, 1–6. [CrossRef] [PubMed]
126. Wang, H.; Wei, C.; Zhu, K.; Zhang, Y.; Gong, C.; Guo, J.; Zhang, J.; Yu, L.; Zhang, J. Preparation of Graphene Sheets by Electrochemical Exfoliation of Graphite in Confined Space and Their Application in Transparent Conductive Films. *ACS Appl. Mater. Interfaces* **2017**, *9*, 34456–34466. [CrossRef] [PubMed]
127. Essig, S.; Allebé, C.; Remo, T.; Geisz, J.F.; Steiner, M.A.; Horowitz, K.; Barraud, L.; Ward, J.S.; Schnabel, M.; Descoeudres, A.; et al. Raising the one-sun conversion efficiency of III-V/Si solar cells to 32.8% for two junctions and 35.9% for three junctions. *Nat. Energy* **2017**, *2*, 17144. [CrossRef]
128. Singh, R.; Charu Tripathi, C. Electrochemical Exfoliation of Graphite into Graphene for Flexible Supercapacitor Application. *Mater. Today Proc.* **2018**, *5*, 1125–1130. [CrossRef]
129. Vartak, R.; Rag, A.; De, S.; Bhat, S. *A Facile Synthesis of Graphene Oxide (GO) and Reduced Graphene Oxide (RGO) by Electrochemical Exfoliation of Battery Electrode*; Springer: Singapore, 2019; ISBN 9789811316425.
130. Komba, N.; Wei, Q.; Zhang, G.; Rosei, F.; Sun, S. Controlled synthesis of graphene via electrochemical route and its use as efficient metal-free catalyst for oxygen reduction. *Appl. Catal. B Environ.* **2019**, *243*, 373–380. [CrossRef]
131. He, D.; Marsden, A.J.; Li, Z.; Zhao, R.; Xue, W.; Bissett, M.A. A single step strategy to fabricate graphene fibres via electrochemical exfoliation for micro-supercapacitor applications. *Electrochim. Acta* **2019**, *299*, 645–653. [CrossRef]
132. Altavilla, C.; Sarno, M.; Ciambelli, P. A Novel Wet Chemistry Approach for the Synthesis of Hybrid 2D Free-Floating Single or Multilayer Nanosheets of MS2@oleylamine (M = Mo, W). *Chem. Mater.* **2011**, *23*, 3879–3885. [CrossRef]
133. Benavente, E.; Ana, M.A.; Mendizabal, F.; Gonzalez, G. Intercalation chemistry of molybdenum disulfide. *Coord. Chem. Rev.* **2002**, *224*, 87–109. [CrossRef]
134. Tao, H.; Zhang, Y.; Gao, Y.; Sun, Z.; Yan, C.; Texter, J. Scalable exfoliation and dispersion of two-dimensional materials-an update. *Phys. Chem. Chem. Phys.* **2017**, *19*, 921–960. [CrossRef]
135. Brent, J.R.; Savjani, N.; Brien, P.O. Synthetic approaches to two-dimensional transition metal dichalcogenide nanosheets. *Prog. Mater. Sci.* **2017**, *89*, 411–478. [CrossRef]
136. Li, H.; Yin, Z.; He, Q.; Li, H.; Huang, X.; Lu, G.; Fam, D.W.H.; Tok, A.I.Y.; Zhang, Q.; Zhang, H. Fabrication of single- and multilayer MoS_2 film-based field-effect transistors for sensing NO at room temperature. *Small* **2012**, *8*, 63–67. [CrossRef] [PubMed]

137. Bernal, M.M.; Milano, D. *Two-Dimensional Nanomaterials via Liquid-Phase Exfoliation: Synthesis, Properties and Applications*; One Central Press (OCP): Cheshire, UK, 2014; pp. 159–185.
138. Sreekumar, K.; Bindhu, B. Aqueous Exfoliation of Molybdenum Disulfide Using Ultrasonication. *Mater. Today Proc.* **2018**, *5*, 13152–13156. [CrossRef]
139. Cai, X.; Luo, Y.; Liu, B.; Cheng, H.M. Preparation of 2D material dispersions and their applications. *Chem. Soc. Rev.* **2018**, *47*, 6224–6266. [CrossRef]
140. De-Mello, G.B.; Smith, L.; Rowley-Neale, S.J.; Gruber, J.; Hutton, S.J.; Banks, C.E. Surfactant-exfoliated 2D molybdenum disulphide (2D-MoS_2): The role of surfactant upon the hydrogen evolution reaction. *RSC Adv.* **2017**, *7*, 36208–36213. [CrossRef]
141. Guo, Z.; Ma, Q.; Xuan, Z.; Du, F.; Zhong, Y. Facile surfactant-assisted synthesis of CTAB-incorporated MoS_2 ultrathin nanosheets for efficient hydrogen evolution. *RSC Adv.* **2016**, *6*, 16730–16735. [CrossRef]
142. Ciesielski, A.; Samorì, P. Graphene via sonication assisted liquid-phase exfoliation. *Chem. Soc. Rev.* **2014**, *43*, 381–398. [CrossRef]
143. Amiri, A.; Naraghi, M.; Ahmadi, G.; Soleymaniha, M.; Shanbedi, M. A review on liquid-phase exfoliation for scalable production of pure graphene, wrinkled, crumpled and functionalized graphene and challenges. *FlatChem* **2018**, *8*, 40–71. [CrossRef]
144. Zhang, J.; Xu, L.; Zhou, B.; Zhu, Y.; Jiang, X. The pristine graphene produced by liquid exfoliation of graphite in mixed solvent and its application to determination of dopamine. *J. Colloid Interface Sci.* **2018**, *513*, 279–286. [CrossRef]
145. Wu, J.Y.; Lai, Y.C.; Chang, C.L.; Hung, W.C.; Wu, H.M.; Liao, Y.C.; Huang, C.H.; Liu, W.R. Facile and green synthesis of graphene-based conductive adhesives via liquid exfoliation process. *Nanomaterials* **2019**, *9*, 38. [CrossRef]
146. Ye, H.; Lu, T.; Xu, C.; Han, B.; Meng, N.; Xu, L. Liquid-Phase Exfoliation of Hexagonal Boron Nitride into Boron Nitride Nanosheets in Common Organic Solvents with Hyperbranched Polyethylene as Stabilizer. *Macromol. Chem. Phys.* **2018**, *219*, 1700482. [CrossRef]
147. Tian, Z.; Chen, K.; Sun, S.; Zhang, J.; Cui, W.; Xie, Z.; Liu, G. Crystalline boron nitride nanosheets by sonication-assisted hydrothermal exfoliation. *J. Adv. Ceram.* **2019**, *8*, 72–78. [CrossRef]
148. Del Rio Castillo, A.E.; Pellegrini, V.; Sun, H.; Buha, J.; Dinh, D.A.; Lago, E.; Ansaldo, A.; Capasso, A.; Manna, L.; Bonaccorso, F. Exfoliation of Few-Layer Black Phosphorus in Low-Boiling-Point Solvents and Its Application in Li-Ion Batteries. *Chem. Mater.* **2018**, *30*, 506–516. [CrossRef]
149. Jia, C.; Zhao, L.; Cui, M.; Yang, F.; Cheng, G.; Yang, G.; Zeng, Z. Surface coordination modification and electrical properties of few-layer black phosphorus exfoliated by the liquid-phase method. *J. Alloys Compd.* **2019**, *799*, 99–107. [CrossRef]
150. Zhao, G.; Wu, Y.; Shao, Y.; Hao, X. Large-quantity and continuous preparation of two-dimensional nanosheets. *Nanoscale* **2016**, *8*, 5407–5411. [CrossRef]
151. Shen, J.; He, Y.; Wu, J.; Gao, C.; Keyshar, K.; Zhang, X.; Yang, Y.; Ye, M.; Vajtai, R.; Lou, J.; et al. Liquid Phase Exfoliation of Two-Dimensional Materials by Directly Probing and Matching Surface Tension Components. *Nano Lett.* **2015**, *15*, 5449–5454. [CrossRef]
152. Gerchman, D.; Alves, A.K. Solution-processable exfoliation and suspension of atomically thin WSe. *J. Colloid Interface Sci.* **2016**, *468*, 247–252. [CrossRef]
153. Hennrich, F.; Krupke, R.; Arnold, K.; Stu, J.A.R.; Lebedkin, S.; Koch, T.; Schimmel, T.; Kappes, M.M. The Mechanism of Cavitation-Induced Scission of Single-Walled Carbon Nanotubes. *J. Phys. Chem* **2007**, *111*, 1932–1937. [CrossRef]
154. Suslick, K.S.; Hammerton, D.A.; Cline, R.E. The Sonochemical Hot Spot. *J. Am. Chem. Soc.* **1986**, *108*, 5641–5642. [CrossRef]
155. Duclaux, L.; Alvarez, L.; Hawełek, Ł. Cleavage and size reduction of graphite crystal using ultrasound radiation. *Carbon N. Y.* **2013**, *55*, 53–61.
156. Han, J.T.; Jang, J.I.; Kim, H.; Hwang, J.Y.; Yoo, H.K.; Woo, J.S.; Choi, S.; Kim, H.Y.; Jeong, H.J.; Jeong, S.Y.; et al. Extremely Efficient Liquid Exfoliation and Dispersion of Layered Materials by Unusual Acoustic Cavitation. *Sci. Rep.* **2014**, *4*, 5133. [CrossRef] [PubMed]
157. Coleman, J.N.; Lotya, M.; O'Neill, A.; Bergin, S.D.; King, P.J.; Khan, U.; Young, K.; Gaucher, A.; De, S.; Smith, R.J. Two-Dimensional Nanosheets Produced by Liquid Exfoliation of Layered Materials. *Science* **2011**, *331*, 568–571. [CrossRef] [PubMed]

158. Bonaccorso, F.; Bartolotta, A.; Coleman, J.N.; Backes, C.; Vi, I.I.I. 2D-Crystal-Based Functional Inks. *Adv. Mater.* **2016**, *28*, 6136–6166. [CrossRef] [PubMed]
159. Zhang, X.; Lai, Z.; Tan, C.; Zhang, H. Solution-Processed Two-Dimensional MoS_2 Nanosheets: Preparation, Hybridization, and Applications. *Angew. Chem. Int. Ed.* **2016**, *55*, 8816–8838. [CrossRef]
160. Backes, C.; Higgins, T.M.; Kelly, A.; Boland, C.; Harvey, A.; Hanlon, D.; Coleman, J.N. Guidelines for exfoliation, characterization and processing of layered materials produced by liquid exfoliation. *Chem. Mater.* **2017**, *29*, 243–255. [CrossRef]
161. Backes, C.; Hanlon, D.; Szydlowska, B.M.; Harvey, A.; Smith, R.J.; Higgins, T.M.; Coleman, J.N. Preparation of Liquid-exfoliated Transition Metal Dichalcogenide Nanosheets with Controlled Size and Thickness: A State of the Art Protocol. *J. Vis. Exp.* **2016**, 1–10. [CrossRef]
162. Cunningham, G.; Lotya, M.; Cucinotta, C.S.; Sanvito, S.; Bergin, S.D.; Menzel, R.; Shaffer, M.S.P.; Coleman, J.N. Solvent exfoliation of transition metal dichalcogenides: Dispersibility of exfoliated nanosheets varies only weakly between compounds. *ACS Nano* **2012**, *6*, 3468–3480. [CrossRef]
163. Huang, J.; Deng, X.; Wan, H.; Chen, F.; Lin, Y.; Xu, X.; Ma, R.; Sasaki, T. Liquid Phase Exfoliation of MoS_2 Assisted by Formamide Solvothermal Treatment and Enhanced Electrocatalytic Activity Based on (H3Mo12O40P/MoS_2)n Multilayer Structure. *ACS Sustain. Chem. Eng.* **2018**, *6*, 5227–5237. [CrossRef]
164. Rathod, N.; Hatzikiriakos, S.G. The effect of surface energy of boron nitride on polymer processability. *Polym. Eng. Sci.* **2004**, *44*, 1543–1550. [CrossRef]
165. O'Neill, A.; Khan, U.; Nirmalraj, P.N.; Boland, J.; Coleman, J.N. Graphene dispersion and exfoliation in low boiling point solvents. *J. Phys. Chem. C* **2011**, *115*, 5422–5428. [CrossRef]
166. Kim, J.; Kwon, S.; Cho, D.-H.; Kang, B.; Kwon, H.; Kim, Y.; Park, S.O.; Jung, G.Y.; Shin, E.; Kim, W.-G.; et al. Direct exfoliation and dispersion of two-dimensional materials in pure water via temperature control. *Nat. Commun.* **2015**, *6*, 8294. [CrossRef] [PubMed]
167. Tang, Z.; Wei, Q.; Guo, B. A generic solvent exchange method to disperse MoS_2 in organic solvents to ease the solution process. *Chem. Commun.* **2014**, *50*, 3934–3937. [CrossRef] [PubMed]
168. Wang, Y.; Yang, R.X.; Quhe, R.; Zhong, H.; Cong, L.; Ye, M.; Ni, Z.; Song, Z.; Yang, J.; Shi, J.; et al. Does p-type ohmic contact exist in WSe2-metal interfaces? *Nanoscale* **2016**, *8*, 1179–1191. [CrossRef] [PubMed]
169. Liu, J.; Zeng, Z.; Cao, X.; Lu, G.; Wang, L.-H.; Fan, Q.-L.; Huang, W.; Zhang, H. Preparation of MoS_2-polyvinylpyrrolidone nanocomposites for flexible nonvolatile rewritable memory devices with reduced graphene oxide electrodes. *Small* **2012**, *8*, 3517–3522. [CrossRef]
170. May, P.; Khan, U.; Hughes, J.M.; Coleman, J.N. Role of solubility parameters in understanding the steric stabilization of exfoliated two-dimensional nanosheets by adsorbed polymers. *J. Phys. Chem. C* **2012**, *116*, 11393–11400. [CrossRef]
171. Bari, R.; Parviz, D.; Khabaz, F.; Klaassen, C.D.; Metzler, S.D.; Hansen, M.J.; Khare, R.; Green, M.J. Liquid phase exfoliation and crumpling of inorganic nanosheets. *Phys. Chem. Chem. Phys.* **2015**, *17*, 9383–9393. [CrossRef]
172. Smith, R.J.; King, P.J.; Lotya, M.; Wirtz, C.; Khan, U.; De, S.; O'Neill, A.; Duesberg, G.S.; Grunlan, J.C.; Moriarty, G.; et al. Large-scale exfoliation of inorganic layered compounds in aqueous surfactant solutions. *Adv. Mater.* **2011**, *23*, 3944–3948. [CrossRef]
173. Štengl, V.; Tolasz, J.; Popelková, D. Ultrasonic preparation of tungsten disulfide single-layers and quantum dots. *RSC Adv.* **2015**, *5*, 89612–89620. [CrossRef]
174. Biccai, S.; Barwich, S.; Boland, D.; Harvey, A.; Hanlon, D.; McEvoy, N.; Coleman, J.N. Exfoliation of 2D materials by high shear mixing. *2D Mater.* **2019**, *6*, 015008. [CrossRef]
175. Tian, J.; Guo, L.; Yin, X.; Wu, W. The liquid-phase preparation of graphene by shear exfoliation with graphite oxide as a dispersant. *Mater. Chem. Phys.* **2019**, *223*, 1–8. [CrossRef]
176. Paton, K.R.; Varrla, E.; Backes, C.; Smith, R.J.; Khan, U.; O'Neill, A.; Boland, C.; Lotya, M.; Istrate, O.M.; King, P.; et al. Scalable production of large quantities of defect-free few-layer graphene by shear exfoliation in liquids. *Nat. Mater.* **2014**, *13*, 624–630. [CrossRef] [PubMed]
177. Varrla, E.; Backes, C.; Paton, K.R.; Harvey, A.; Gholamvand, Z.; McCauley, J.; Coleman, J.N. Large-Scale Production of Size-Controlled MoS_2 Nanosheets by Shear Exfoliation. *Chem. Mater.* **2015**, *27*, 1129–1139. [CrossRef]
178. Xu, F.; Ge, B.; Chen, J.; Nathan, A.; Xin, L.L.; Ma, H.; Min, H.; Zhu, C.; Xia, W.; Li, Z.; et al. Scalable shear-exfoliation of high-quality phosphorene nanoflakes with reliable electrochemical cycleability in nano batteries. *2D Mater.* **2016**, *3*, 1–12. [CrossRef]

179. Heising, J.; Kanatzidis, M.G. Exfoliated and Restacked MoS_2 and WS_2: Ionic or Neutral Species? Encapsulation and Ordering of Hard Electropositive Cations. *J. Am. Chem. Soc.* **1999**, *121*, 11720–11732. [CrossRef]
180. Liang, W.Y. Electronic Properties of Transition Metal Dichalcogenides and Their Intercalation Complexes. In *Intercalation in Layered Materials*; Springer: Berlin/Heidelberg, Germany, 1986; pp. 31–73.
181. Koike, Y.; Tanuma, S.I.; Suematsu, H.; Higuchi, K. Superconductivity in the graphite-potassium intercalation compound C8K. *Solid State Commun.* **1978**, *27*, 623–627. [CrossRef]
182. Joensen, P.; Frindt, R.F.; Morrison, S.R. Single-layer MoS. *Mater. Res. Bull.* **1986**, *21*, 457–461. [CrossRef]
183. Eng, A.Y.S.; Ambrosi, A.; Sofer, Z.; Šimek, P.; Pumera, M. Electrochemistry of transition metal dichalcogenides: Strong dependence on the metal-to-chalcogen composition and exfoliation method. *ACS Nano* **2014**, *8*, 12185–12198. [CrossRef]
184. Ambrosi, A.; Sofer, Z.; Pumera, M. Lithium intercalation compound dramatically influences the electrochemical properties of exfoliated MoS. *Small* **2015**, *11*, 605–612. [CrossRef]
185. Murphy, D.W.; Di Salvo, F.J.; Hull, G.W.; Waszczak, J. V Convenient preparation and physical properties of lithium intercalation compounds of Group 4B and 5B layered transition metal dichalcogenides. *Inorg. Chem.* **1976**, *15*, 17–21. [CrossRef]
186. Eda, G.; Fujita, T.; Yamaguchi, H.; Voiry, D.; Chen, M.; Chhowalla, M. Coherent Atomic and Electronic Heterostructures of Single-Layer MoS_2. *ACS Nano* **2012**, *6*, 7311–7317. [CrossRef]
187. Fujita, T.; Ito, Y.; Tan, Y.; Yamaguchi, H.; Hojo, D.; Hirata, A.; Voiry, D.; Chhowalla, M.; Chen, M. Chemically exfoliated ReS2 nanosheets. *Nanoscale* **2014**, *6*, 12458–12462. [CrossRef] [PubMed]
188. Ambrosi, A.; Sofer, Z.; Pumera, M. 2H-1T phase transition and hydrogen evolution activity of MoS_2, MoSe2, WS_2 and WSe2 strongly depends on the MX2 composition. *Chem. Commun.* **2015**, *51*, 8450–8453. [CrossRef] [PubMed]
189. Fan, X.; Xu, P.; Zhou, D.; Sun, Y.; Li, Y.C.; Nguyen, M.A.T.; Terrones, M.; Mallouk, T.E. Fast and Efficient Preparation of Exfoliated 2H MoS_2 Nanosheets by Sonication-Assisted Lithium Intercalation and Infrared Laser-Induced 1T to 2H Phase Reversion. *Nano Lett.* **2015**, *15*, 5956–5960. [CrossRef] [PubMed]
190. Lukowski, M.A.; Daniel, A.S.; English, C.R.; Meng, F.; Forticaux, A.; Hamers, R.J.; Jin, S. Highly active hydrogen evolution catalysis from metallic WS_2 nanosheets. *Energy Environ. Sci.* **2014**, *7*, 2608–2613. [CrossRef]
191. Ramakrishna Matte, H.S.S.; Gomathi, A.; Manna, A.K.; Late, D.J.; Datta, R.; Pati, S.K.; Rao, C.N.R. MoS_2 and WS_2 analogues of graphene. *Angew. Chem. Int. Ed.* **2010**, *49*, 4059–4062. [CrossRef]
192. Yuwen, L.; Yu, H.; Yang, X.; Zhou, J.; Zhang, Q.; Zhang, Y.; Luo, Z.; Su, S.; Wang, L. Rapid preparation of single-layer transition metal dichalcogenide nanosheets via ultrasonication enhanced lithium intercalation. *Chem. Commun.* **2016**, *52*, 529–532. [CrossRef]
193. Giacometti, V.; Radisavljevic, B.; Radenovic, A.; Brivio, J.; Kis, A.; Giacometti, V.; Kis, A. Single-layer MoS_2 transistors. *Nat. Nanotechnol.* **2011**, *6*, 147–150.
194. Jeong, S.; Yoo, D.; Ahn, M.; Miro, P.; Heine, T.; Cheon, J. Tandem intercalation strategy for single-layer nanosheets as an effective alternative to conventional exfoliation processes. *Nat. Commun.* **2015**, *6*, 1–7. [CrossRef]
195. Cullen, P.L.; Cox, K.M.; Bin Subhan, M.K.; Picco, L.; Payton, O.D.; Buckley, D.J.; Miller, T.S.; Hodge, S.A.; Skipper, N.T.; Tileli, V.; et al. Ionic solutions of two-dimensional materials. *Nat. Chem.* **2017**, *9*, 244–249. [CrossRef]
196. Anto Jeffery, A.; Nethravathi, C.; Rajamathi, M. Two-dimensional nanosheets and layered hybrids of MoS_2 and WS_2 through exfoliation of ammoniated MS2 (M = Mo, W). *J. Phys. Chem. C* **2014**, *118*, 1386–1396. [CrossRef]
197. Liu, G.; Ma, H.; Teixeira, I.; Sun, Z.; Xia, Q.; Hong, X.; Tsang, S.C.E. Hydrazine-Assisted Liquid Exfoliation of MoS_2 for Catalytic Hydrodeoxygenation of 4-Methylphenol. *Chem. Eur. J.* **2016**, *22*, 2910–2914. [CrossRef]
198. Bang, G.S.; Nam, K.W.; Kim, J.Y.; Shin, J.; Choi, J.W.; Choi, S.-Y. Effective liquid-phase exfoliation and sodium ion battery application of MoS_2 nanosheets. *ACS Appl. Mater. Interfaces* **2014**, *6*, 7084–7089. [CrossRef] [PubMed]
199. Zeng, Z.; Yin, Z.; Huang, X.; Li, H.; He, Q.; Lu, G.; Boey, F.; Zhang, H. Single-layer semiconducting nanosheets: High-yield preparation and device fabrication. *Angew. Chem. Int. Ed.* **2011**, *50*, 11093–11097. [CrossRef] [PubMed]

200. You, X.; Liu, N.; Lee, C.J.; Jungho, J. An electrochemical route to MoS 2 nanosheets for device applications. *Mater. Lett.* **2014**, *121*, 31–35. [CrossRef]
201. Liu, N.; Kim, P.; Kim, J.H.; Ye, J.H.; Kim, S.; Lee, C.J. Large-area atomically thin MoS_2 nanosheets prepared using electrochemical exfoliation. *ACS Nano* **2014**, *8*, 6902–6910. [CrossRef]
202. Ambrosi, A.; Pumera, M. Exfoliation of layered materials using electrochemistry. *Chem. Soc. Rev.* **2018**, *47*, 7213–7224. [CrossRef] [PubMed]
203. Lin, Z.; Liu, Y.; Halim, U.; Ding, M.; Liu, Y.; Wang, Y.; Jia, C.; Chen, P.; Duan, X.; Wang, C.; et al. Solution-processable 2D semiconductors for high-performance large-area electronics. *Nature* **2018**, *562*, 254–258. [CrossRef]
204. Li, F.; Xue, M.; Zhang, X.; Chen, L.; Knowles, G.P.; MacFarlane, D.R.; Zhang, J. Advanced Composite 2D Energy Materials by Simultaneous Anodic and Cathodic Exfoliation. *Adv. Energy Mater.* **2018**, *8*, 1–8. [CrossRef]
205. Das, S.; Pandey, D.; Thomas, J.; Roy, T. The Role of Graphene and Other 2D Materials in Solar Photovoltaics. *Adv. Mater.* **2019**, *31*, 1–35. [CrossRef]
206. Yu, X.; Sivula, K. Toward Large-Area Solar Energy Conversion with Semiconducting 2D Transition Metal Dichalcogenides. *ACS Energy Lett.* **2016**, *1*, 315–322. [CrossRef]
207. Khan, M.A.; Leuenberger, M.N. Optoelectronics with single layer group-VIB transition metal dichalcogenides. *Nanophotonics* **2018**, *7*, 1589–1600. [CrossRef]
208. Akama, T.; Okita, W.; Nagai, R.; Li, C.; Kaneko, T.; Kato, T. Schottky solar cell using few-layered transition metal dichalcogenides toward large-scale fabrication of semitransparent and flexible power generator. *Sci. Rep.* **2017**, *7*, 1–10. [CrossRef]
209. Singh, E.; Kim, K.S.; Yeom, G.Y.; Nalwa, H.S. Atomically thin-layered molybdenum disulfide (MoS_2) for bulk-heterojunction solar cells. *ACS Appl. Mater. Interfaces* **2017**, *9*, 3223–3245. [CrossRef] [PubMed]
210. Tang, W.; Rassay, S.S.; Ravindra, N.M. Electronic & Optical properties of Transition-Metal Dichalcogenides. *Madr. J. Nanotechnol. Nanosci.* **2017**, *2*, 58–64.
211. Bernardi, M.; Palummo, M.; Grossman, J.C. Extraordinary sunlight absorption and one nanometer thick photovoltaics using two-dimensional monolayer materials. *Nano Lett.* **2013**, *13*, 3664–3670. [CrossRef] [PubMed]
212. Dou, Y.Y.; Li, G.R.; Song, J.; Gao, X.P. Nickel phosphide-embedded graphene as counter electrode for dye-sensitized solar cells. *Phys. Chem. Chem. Phys.* **2012**, *14*, 1339–1342. [CrossRef] [PubMed]
213. Jeong, H.; Jae-Yup, K.; Koo, B.; Son, H.; Kim, D.; Ko, M. Rapid sintering of MoS_2 counter electrode using near-infrared pulsed laser for use in highly efficient dye-sensitized solar cells. *J. Power Sources* **2016**, *330*, 104–110. [CrossRef]
214. Antonelou, A.; Syrrokostas, G.; Sygellou, L.; Leftheriotis, G.; Dracopoulos, V.; Yannopoulos, S. Facile, substrate-scale growth of mono- and few-layer homogeneous MoS_2 films on Mo foils with enhanced catalytic activity as counter electrodes in DSSCs. *Nanotechnology* **2015**, *27*, 45404. [CrossRef]
215. Cheng, C.K.; Hsieh, C.K. Electrochemical deposition of molybdenum sulfide thin films on conductive plastic substrates as platinum-free flexible counter electrodes for dye-sensitized solar cells. *Thin Solid Films* **2015**, *584*, 52–60. [CrossRef]
216. Lei, B.; Li, G.R.; Gao, X.P. Morphology dependence of molybdenum disulfide transparent counter electrode in dye-sensitized solar cells. *J. Mater. Chem. A* **2014**, *2*, 3919–3925. [CrossRef]
217. Lin, J.-Y.; Yue, G.; Tai, S.-Y.; Xiao, Y.; Cheng, H.-M.; Wang, F.-M.; Wu, J. Hydrothermal synthesis of graphene flake embedded nanosheet-like molybdenum sulfide hybrids as counter electrode catalysts for dye-sensitized solar cells. *Mater. Chem. Phys.* **2013**, *143*, 53–59. [CrossRef]
218. Liu, C.-J.; Tai, S.-Y.; Chou, S.-W.; Yu, Y.-C.; Chang, K.-D.; Wang, S.; Chien, F.S.-S.; Lin, J.-Y.; Lin, T.-W. Facile synthesis of MoS_2/graphene nanocomposite with high catalytic activity toward triiodide reduction in dye-sensitized solar cells. *J. Mater. Chem.* **2012**, *22*, 21057–21064. [CrossRef]
219. Balis, N.; Stratakis, E.; Kymakis, E. Graphene and transition metal dichalcogenide nanosheets as charge transport layers for solution processed solar cells. *Biochem. Pharmacol.* **2016**, *19*, 580–594. [CrossRef]
220. Kakavelakis, G.; Gouda, L.; Tischler, Y.; Kaliakatsos, I.; Petridis, K. *2D Transition Metal Dichalcogenides for Solution-Processed Organic and Perovskite Solar Cells*; Springer: Singapore, 2019; ISBN 9789811390456.

221. Gu, X.; Cui, W.; Li, H.; Wu, Z.; Zeng, Z.; Lee, S.T.; Zhang, H.; Sun, B. A solution-processed hole extraction layer made from ultrathin MoS_2 nanosheets for efficient organic solar cells. *Adv. Energy Mater.* **2013**, *3*, 1262–1268. [CrossRef]
222. Li, X.; Zhang, W.; Wu, Y.; Min, C.; Fang, J. Solution-Processed MoSx as an Efficient Anode Buffer Layer in Organic Solar Cells. *ACS Appl. Mater. Interfaces* **2013**, *5*, 8823–8827. [CrossRef]
223. Ramasamy, M.S.; Ryu, K.Y.; Lim, J.W.; Bibi, A.; Kwon, H.; Lee, J.E.; Kim, D.H.; Kim, K. Solution-processed PEDOT: PSS/MoS_2 nanocomposites as efficient hole-transporting layers for organic solar cells. *Nanomaterials* **2019**, *9*, 1328. [CrossRef]
224. Yang, X.; Fu, W.; Liu, W.; Hong, J.; Cai, Y.; Jin, C.; Xu, M.; Wang, H.; Yang, D.; Chen, H. Engineering crystalline structures of two-dimensional MoS_2 sheets for high-performance organic solar cells. *J. Mater. Chem. A* **2014**, *2*, 7727–7733. [CrossRef]
225. Yun, J.-M.; Noh, Y.-J.; Yeo, J.-S.; Go, Y.-J.; Na, S.-I.; Jeong, H.-G.; Kim, J.; Lee, S.; Kim, S.-S.; Koo, H.Y.; et al. Efficient work-function engineering of solution-processed MoS_2 thin-films for novel hole and electron transport layers leading to high-performance polymer solar cells. *J. Mater. Chem. C* **2013**, *1*, 3777–3783. [CrossRef]
226. Hu, X.; Chen, L.; Tan, L.; Zhang, Y.; Hu, L.; Xie, B.; Chen, Y. Versatile MoS_2 Nanosheets in ITO-Free and Semi-transparent Polymer Power-generating Glass. *Sci. Rep.* **2015**, *5*, 1–13. [CrossRef]
227. Qin, P.; Fang, G.; Ke, W.; Cheng, F.; Zheng, Q.; Wan, J.; Lei, H.; Zhao, X. In situ growth of double-layer MoO3/MoS_2 film from MoS_2 for hole-transport layers in organic solar cell. *J. Mater. Chem. A* **2014**, *2*, 2742–2756. [CrossRef]
228. Yang, X.; Liu, W.; Xiong, M.; Zhang, Y.; Liang, T.; Yang, J.; Xu, M.; Ye, J.; Chen, H. Au nanoparticles on ultrathin MoS_2 sheets for plasmonic organic solar cells. *J. Mater. Chem. A* **2014**, *2*, 14798–14806. [CrossRef]
229. Chuang, M.K.; Yang, S.S.; Chen, F.C. Metal nanoparticle-decorated two-dimensional molybdenum sulfide for plasmonic-enhanced polymer photovoltaic devices. *Materials (Basel)* **2015**, *8*, 5414–5425. [CrossRef] [PubMed]
230. Wang, Y.; Wang, S.; Chen, X.; Li, Z.; Wang, J.; Li, T.; Deng, X. Largely enhanced VOC and stability in perovskite solar cells with modified energy match by coupled 2D interlayers. *J. Mater. Chem. A* **2018**, *6*, 4860–4867. [CrossRef]
231. Tsai, M.L.; Su, S.H.; Chang, J.K.; Tsai, D.S.; Chen, C.H.; Wu, C.I.; Li, L.J.; Chen, L.J.; He, J.H. Monolayer MoS_2 heterojunction solar cells. *ACS Nano* **2014**, *8*, 8317–8322. [CrossRef] [PubMed]
232. Zhou, D.; Zhou, T.; Tian, Y.; Zhu, X.; Tu, Y. Perovskite-Based Solar Cells: Materials, Methods, and Future Perspectives. *J. Nanomater.* **2018**, *2018*, 8148072. [CrossRef]
233. Zhou, P.; Bu, T.; Shi, S.; Li, L.; Zhang, Y.; Ku, Z.; Peng, Y.; Zhong, J.; Cheng, Y.-B.; Huang, F. Efficient and stable mixed perovskite solar cells using P3HT as a hole transporting layer. *J. Mater. Chem. C* **2018**, *6*, 5733–5737. [CrossRef]
234. Yang, Q.-D.; Li, J.; Cheng, Y.; Li, H.-W.; Guan, Z.; Yu, B.; Tsang, S.-W. Graphene oxide as an efficient hole-transporting material for high-performance perovskite solar cells with enhanced stability. *J. Mater. Chem. A* **2017**, *5*, 9852–9858. [CrossRef]
235. Wang, C.; Zhang, C.; Tong, S.; Xia, H.; Wang, L.; Xie, H.; Gao, Y.; Yang, J. Energy level and thickness control on PEDOT:PSS layer for efficient planar heterojunction perovskite cells. *J. Phys. D Appl. Phys.* **2018**, *51*, 025110. [CrossRef]
236. Sahoo, S.; Tiwari, S.K.; Nayak, G.C. *Surface Engineering of Graphene*; Springer: Berlin/Heidelberg, Germany, 2019.
237. Palma, A.L.; Cinà, L.; Pescetelli, S.; Agresti, A.; Raggio, M.; Paolesse, R.; Bonaccorso, F.; Di Carlo, A. Reduced graphene oxide as efficient and stable hole transporting material in mesoscopic perovskite solar cells. *Nano Energy* **2016**, *22*, 349–360. [CrossRef]
238. Uthayaraj, S.; Karunarathne, D.G.B.C.; Kumara, G.R.A. Powder Pressed Cuprous Iodide (CuI) as A Hole Transporting Material for Perovskite Solar Cells. *Materials (Basel)* **2019**, *12*, 2037. [CrossRef]
239. Dasgupta, U.; Chatterjee, S.; Pal, A.J. Thin-film formation of 2D MoS_2 and its application as a hole-transport layer in planar perovskite solar cells. *Sol. Energy Mater. Sol. Cells* **2017**, *172*, 353–360. [CrossRef]
240. Kim, Y.G.; Kwon, K.C.; Van Le, Q.; Hong, K.; Jang, H.W.; Kim, S.Y. Atomically thin two-dimensional materials as hole extraction layers in organolead halide perovskite photovoltaic cells. *J. Power Sources* **2016**, *319*, 1–8. [CrossRef]

241. Capasso, A.; Del Rio Castillo, A.E.; Najafi, L.; Pellegrini, V.; Bonaccorso, F.; Matteocci, F.; Cina, L.; Di Carlo, A. Spray deposition of exfoliated MoS_2 flakes as hole transport layer in perovskite-based photovoltaics. In Proceedings of the IEEE-NANO 2015—15th International Conference on Nanotechnology; Institute of Electrical and Electronics Engineers Inc.: Piscataway, NJ, USA, 2015; pp. 1138–1141.
242. Capasso, A.; Matteocci, F.; Najafi, L.; Prato, M.; Buha, J.; Cinà, L.; Pellegrini, V.; Di Carlo, A.; Bonaccorso, F. Few-Layer MoS_2 Flakes as Active Buffer Layer for Stable Perovskite Solar Cells. *Adv. Energy Mater.* **2016**, *6*, 1600920. [CrossRef]
243. Huang, P.; Wang, Z.; Liu, Y.; Zhang, K.; Yuan, L.; Zhou, Y.; Song, B.; Li, Y. Water-Soluble 2D Transition Metal Dichalcogenides as the Hole-Transport Layer for Highly Efficient and Stable p–i–n Perovskite Solar Cells. *ACS Appl. Mater. Interfaces* **2017**, *9*, 25323–25331. [CrossRef] [PubMed]
244. Kakavelakis, G.; Paradisanos, I.; Paci, B.; Generosi, A.; Papachatzakis, M.; Maksudov, T.; Najafi, L.; Del Rio Castillo, A.E.; Kioseoglou, G.; Stratakis, E.; et al. Extending the Continuous Operating Lifetime of Perovskite Solar Cells with a Molybdenum Disulfide Hole Extraction Interlayer. *Adv. Energy Mater.* **2018**, *8*, 1702287. [CrossRef]
245. Kohnehpoushi, S.; Nazari, P.; Nejand, B.A.; Eskandari, M. MoS_2: A two-dimensional hole-transporting material for high-efficiency, low-cost perovskite solar cells. *Nanotechnology* **2018**, *29*, 205201. [CrossRef]
246. Narayanasamy Sabari Arul, V.D.N. *Two Dimensional Transition Metal Dichalcogenides: Synthesis, Properties and Applications*; Springer: Berlin/Heidelberg, Germany, 2019.
247. Mak, K.F.; Shan, J. Photonics and optoelectronics of 2D semiconductor transition metal dichalcogenides. *Nat. Photonics* **2016**, *10*, 216–226. [CrossRef]
248. Yu, W.J.; Vu, Q.A.; Oh, H.; Nam, H.G.; Zhou, H.; Cha, S.; Kim, J.Y.; Carvalho, A.; Jeong, M.; Choi, H.; et al. Unusually efficient photocurrent extraction in monolayer van der Waals heterostructure by tunnelling through discretized barriers. *Nat. Commun.* **2016**, *7*, 1–9. [CrossRef]
249. Lee, J.Y.; Shin, J.H.; Lee, G.H.; Lee, C.H. Two-dimensional semiconductor optoelectronics based on van der Waals heterostructures. *Nanomaterials* **2016**, *6*, 193. [CrossRef]
250. Pradhan, N.R.; Talapatra, S.; Terrones, M.; Ajayan, P.M.; Balicas, L. Optoelectronic Properties of Heterostructures: The Most Recent Developments Based on Graphene and Transition-Metal Dichalcogenides. *IEEE Nanotechnol. Mag.* **2017**, *11*, 18–32. [CrossRef]
251. Wirth-Lima, A.J.; Alves-Sousa, P.P.; Bezerra-Fraga, W. Graphene/silicon and 2D-MoS_2/silicon solar cells: A review. *Appl. Phys. A Mater. Sci. Process.* **2019**, *125*, 241. [CrossRef]
252. Ma, J.; Bai, H.; Zhao, W.; Yuan, Y.; Zhang, K. High efficiency graphene/MoS_2/Si Schottky barrier solar cells using layer-controlled MoS_2 films. *Sol. Energy* **2018**, *160*, 76–84. [CrossRef]
253. Hao, L.; Liu, Y.; Gao, W.; Han, Z.; Xue, Q.; Zeng, H.; Wu, Z.; Zhu, J.; Zhang, W. Electrical and photovoltaic characteristics of MoS_2/Si p-n junctions. *J. Appl. Phys.* **2015**, *117*, 114502. [CrossRef]
254. Hasani, A.; Van Le, Q.; Tekalgne, M.; Choi, M.J.; Lee, T.H.; Kim, S.Y.; Jang, H.W. Direct synthesis of two-dimensional MoS_2 on p-type Si and application to solar hydrogen production. *NPG Asia Mater.* **2019**, *11*, 1–9. [CrossRef]
255. Jiao, K.; Duan, C.; Wu, X.; Chen, J.; Wang, Y.; Chen, Y. The role of MoS_2 as an interfacial layer in graphene/silicon solar cells. *Phys. Chem. Chem. Phys.* **2015**, *17*, 8182–8186. [CrossRef]
256. Hao, L.Z.; Gao, W.; Liu, Y.J.; Han, Z.D.; Xue, Q.Z.; Guo, W.Y.; Zhu, J.; Li, Y.R. High-performance n-MoS_2/i-SiO2/p-Si heterojunction solar cells. *Nanoscale* **2015**, *7*, 8304–8308. [CrossRef]
257. Tsuboi, Y.; Wang, F.; Kozawa, D.; Funahashi, K.; Mouri, S.; Miyauchi, Y.; Takenobu, T.; Matsuda, K. Enhanced photovoltaic performances of graphene/Si solar cells by insertion of a MoS_2 thin film. *Nanoscale* **2015**, *7*, 14476–14482. [CrossRef]
258. Furchi, M.M.; Pospischil, A.; Libisch, F.; Burgdörfer, J.; Mueller, T. Photovoltaic Effect in an Electrically Tunable van der Waals Heterojunction. *Nano Lett.* **2014**, *14*, 4785–4791. [CrossRef]
259. Zan, R.; Ramasse, Q.M.; Jalil, R.; Tu, J.S.; Bangert, U.; Novoselov, K.S. Imaging Two Dimensional Materials and their Heterostructures. *J. Phys. Conf. Ser.* **2017**, *902*, 012028. [CrossRef]
260. Kim, Y.; Choi, D.; Woo, W.J.; Lee, J.B.; Ryu, G.H.; Lim, J.H.; Lee, S.; Lee, Z.; Im, S.; Ahn, J.H.; et al. Synthesis of two-dimensional MoS_2/graphene heterostructure by atomic layer deposition using MoF6 precursor. *Appl. Surf. Sci.* **2019**, *494*, 591–599. [CrossRef]

261. Lee, J.B.; Lim, Y.R.; Katiyar, A.K.; Song, W.; Lim, J.; Bae, S.; Kim, T.W.; Lee, S.K.; Ahn, J.H. Direct Synthesis of a Self-Assembled WSe2/MoS_2 Heterostructure Array and its Optoelectrical Properties. *Adv. Mater.* **2019**, *31*, 1–9.
262. Yang, W.; Kawai, H.; Bosman, M.; Tang, B.; Chai, J.; Le Tay, W.; Yang, J.; Seng, H.L.; Zhu, H.; Gong, H.; et al. Interlayer interactions in 2D WS_2/MoS_2 heterostructures monolithically grown by: In situ physical vapor deposition. *Nanoscale* **2018**, *10*, 22927–22936. [CrossRef] [PubMed]
263. Yan, J.; Ma, C.; Huang, Y.; Yang, G. Tunable Control of Interlayer Excitons in WS_2/MoS_2 Heterostructures via Strong Coupling with Enhanced Mie Resonances. *Adv. Sci.* **2019**, *6*, 1802092. [CrossRef] [PubMed]
264. Rehman, A.U.; Khan, M.F.; Shehzad, M.A.; Hussain, S.; Bhopal, M.F.; Lee, S.H.; Eom, J.; Seo, Y.; Jung, J.; Lee, S.H. N-MoS_2/p-Si Solar Cells with Al_2O_3 Passivation for Enhanced Photogeneration. *ACS Appl. Mater. Interfaces* **2016**, *8*, 29383–29390. [CrossRef] [PubMed]
265. Xu, H.; Xin, L.; Liu, L.; Pang, D.; Jiao, Y.; Cong, R.; Yu, W. Large area MoS_2/Si heterojunction-based solar cell through sol-gel method. *Mater. Lett.* **2019**, *238*, 13–16. [CrossRef]
266. bin Mohd Yusoff, A.R.; Kim, D.; Schneider, F.K.; da Silva, W.J.; Jang, J. Au-doped single layer graphene nanoribbons for a record-high efficiency ITO-free tandem polymer solar cell. *Energy Environ. Sci.* **2015**, *8*, 1523–1537. [CrossRef]
267. Saraswat, K.C.; Park, J.H.; Islam, R.; Nazif, K.N.; Elder, E.; Associate, L. *Low Cost Silicon (Si)/Transition Metal Dichalcogenides (TMDs) Tandem Solar Cells with goal of >30% Efficiency*; Stanford Univ.: Stanford, CA, USA, 2019; Volume S18-187, pp. 1–2.